

Extended-soft-core baryon-baryon model. II. Hyperon-nucleon interaction

Th. A. Rijken

Institute of Mathematics, Astrophysics, and Particle Physics Radboud University, Nijmegen, The Netherlands

Y. Yamamoto

Physics Section, Tsuru University, Tsuru, Yamanashi 402-8555, Japan

(Received 17 October 2005; published 14 April 2006)

The YN results are presented from the extended soft-core (ESC) interactions. They consist of local and nonlocal potentials because of (i) one-boson exchanges (OBE), which are the members of nonets of pseudoscalar, vector, scalar, and axial mesons; (ii) diffractive exchanges; (iii) two-pseudoscalar exchange; and (iv) meson-pair exchange (MPE). Both the OBE and pair vertices are regulated by Gaussian form factors producing potentials with a soft behavior near the origin. The assignment of the cutoff masses for the baryon-baryon-meson (BBM) vertices is dependent on the SU(3) classification of the exchanged mesons for OBE and a similar scheme for MPE. The particular version of the ESC model, called ESC04 [T. A. Rijken, Phys. Rev. C **73**, 044007 (2006)], describes nucleon-nucleon (NN) and hyperon-nucleon (YN) interactions in a unified way using broken SU(3) symmetry. Novel ingredients are the inclusion of (i) the axial-vector meson potentials and (ii) a zero in the scalar- and axial-vector meson form factors. These innovations made it possible for the first time to keep the parameters of the model close to the predictions of the 3P_0 quark-antiquark creation model. This is also the case for the $F/(F+D)$ ratios. Furthermore, the introduction of the zero helped to avoid the occurrence of unwanted bound states. Broken SU(3) symmetry serves to connect the NN and the YN channels, which leaves after fitting NN only a few free parameters for the determination of the YN interactions. In particular, the meson-baryon coupling constants are calculated via SU(3) using the coupling constants of the NN analysis as input. Here, as a novel feature, medium-strong flavor-symmetry breaking (FSB) of the coupling constants was allowed, using the 3P_0 model with a Gell-Mann-Okubo hypercharge breaking for the BBM coupling. Very good fits for ESC model with and without FSB were obtained. The charge-symmetry breaking in the Λp and Λn channels, which is an SU(2) isospin breaking, is included in the OBE, TME, and MPE potentials. Simultaneous fits to the NN - and the YN -scattering data are described, using different options for the ESC model. For the selected 4233 NN data with energies $0 \leq T_{\text{lab}} \leq 350$ MeV, a $\chi^2/N_{\text{data}} = 1.22$ was typically reached. For the usual set of 35 YN data and 3 $\Sigma^+ p$ cross sections from a recent KEK experiment E289 $\chi^2/YN_{\text{data}} \approx 0.63$ was obtained. In particular, we were able to fit the precise experimental datum $r_R = 0.468 \pm 0.010$ for the inelastic capture ratio at rest rather well. The four versions (a,b,c, and d) of ESC04 presented in this article, give different results for hypernuclei. The reported G -matrix calculations are performed for YN (ΛN , ΣN , ΞN) pairs in nuclear matter. The obtained well depths (U_Λ , U_Σ , U_Ξ) reveal distinct features of ESC04a-d. The $\Lambda\Lambda$ interactions are demonstrated to be consistent with the observed data of ${}^6_{\Lambda\Lambda}\text{He}$. The possible three-body effects are investigated by considering phenomenologically the changes of the vector-meson masses.

DOI: [10.1103/PhysRevC.73.044008](https://doi.org/10.1103/PhysRevC.73.044008)

PACS number(s): 21.30.-x, 13.75.Ev, 13.75.Cs, 12.39.Pn

I. INTRODUCTION

This is the second in a series of articles where we present the recent results obtained with the extended soft-core model, henceforth referred to as ESC04, model for nucleon-nucleon (NN), hyperon-nucleon (YN), and hyperon-hyperon (YY). This article treats the NN and YN ($S = -1$) systems. In Ref. [1], in the following referred to as I, many formal aspects have been described or discussed rather extensively. Therefore, in this article we will concentrate on items that are in particularly important in YN and that were not treated in [1]. In part III [2] the $S = -2$ channels are described.

In Refs. [3] and [4] it has been shown the a soft-core (SC) one-boson-exchange (OBE) model, based on Regge-pole theory [5], provides a satisfactory description of many aspects of the nucleon-nucleon (NN) and hyperon-nucleon (YN) channels.

Because for NN the ESC model has provided a big step forward in the detailed description, one may expect that a simultaneous and unified treatment of the NN and YN channels, using broken SU(3), will give a very realistic model for the baryon-baryon interactions. [In this article by SU(3) always refers to SU(3) flavor.]

In all previous work of the Nijmegen group, the exploration of (broken) SU(3) symmetry connects the NN and the YN channels, leaving after fitting NN only a few free parameters to be determined in the YN interactions. The latter is important in view of the scarce experimental YN data. In particular, the baryon-baryon-meson (BBM) coupling constants are calculated via SU(3) using the coupling constants of the NN analysis as input. The first versions of the ESC model, referred to as ESC00 [6,7], worked along the same procedures. The aim of the ESC00 work was to demonstrate the ability of the ESC model to provide a good description of the NN and

YN data, i.e., a low χ^2 . Therefore, we left much freedom to the parameters. However, in the ESC04 version presented here, we focus on the improvement of the physics of the model by restricting the coupling constants in the BBM vertices by the predictions of the quark model (QM) in the form of the 3P_0 antiquark-quark pair creation model (QPC) [8]. Also, all $\alpha = F/(F + D)$ ratios are taken close to the QPC model predictions for the BBM and the BB pair vertices. An exception is made here for the pseudoscalar α_{PV} and the α_V^m ratios. The first because it is interesting to see how close or different it becomes as compared to the same ratio in weak interactions, where $\alpha_{PV} = 0.355$. The second, because it proved to be an important regulator for the S -wave spin dependence of the ΛN interaction [4].

In Ref. [3] the magnetic ratio α_V^m for the vector-mesons was fixed to its SU(6) value, but the spin-spin interaction needed a correction. This because the S -wave spin-spin interaction in the ΛN channels became later well known from hypernuclear systems [9–11]. In Ref. [4], to improve the spin-spin interaction, we left α_V^m free and made fits for different values of this parameter. It turned out that in this way we indeed can construct soft-core YN models that encompass a range of scattering length's in the 1S_0 and the 3S_1 ΛN channels. From the NSC97a-f models the sensitivity with respect to α_V^m is evident.

SU(3) symmetry and the QPC-model give strong constraints on the coupling parameters. To keep some more flexibility in distinguishing the NN and the $YN(S = -1)$ channels, similarly to the NSC97 models [4], we allow for medium strong breaking of the coupling constants, employing again the 3P_0 model with a Gell-Mann-Okubo hypercharge breaking for the BBM coupling. This leads to a universal scheme for SU(3) breaking of the coupling constants for all meson nonets, in terms of a single extra parameter.

To summarize the different sources of SU(3) breaking, we include (i) using the physical masses of the mesons and baryons in the potentials and Schrödinger equation, (ii) allowing for meson mixing within a nonet ($\eta - \eta'$, $\omega - \phi$, $\varepsilon - f'_0$), (iii) including charge symmetry breaking CSB [12] because of $\Lambda\Sigma$ mixing, which, for example, introduces a one-pion-exchange (OPE) potential in the ΛN channel, (iv) taking into account the Coulomb interaction.

The electromagnetic SU(2) breaking [12], called CSB, in the Λp and Λn channels is included, not only for the BBM but also for the BB pair couplings.

The BBM vertices are described by coupling constants and form factors, which correspond to the Regge residues at high energies [5]. The form factors are taken to be of the Gaussian type, like the residue functions in many Regge-pole models for high energy scattering. Note that also in (nonrelativistic) quark models (QMs) a Gaussian behavior of the form factors is most natural. These form factors evidently guarantee a soft behavior of the potentials in configuration space at small distances.

In Ref. [4] the assignment of the cutoff parameters in the form factors was made for the individual BBM vertices, constrained by broken SU(3) symmetry. This in distinction to the first attempt to construct soft-core interaction [3], where cutoffs were assigned per baryon-baryon SU(3)-irrep. The

latter scheme we consider now not natural and we use here the same scheme as in Ref. [4]. Moreover, this way we obtain immediately full predictive power for the $S = -2$, etc., baryon-baryon channels, e.g., $\Lambda\Lambda$, ΞN channels that involve the singlet $\{1\}$ -irrep that does not occur in the NN and YN channels.

The dynamics of the ESC04 model has been described and discussed in part I [1], and it is sufficient to refer to this here for all types of exchanges that are included. Nevertheless, some more remarks on the scalar mesons are appropriate. An extensive discussion of the situation with respect to the scalar mesons is given in Ref. [4]. The question whether the $J^{PC} = 0^{++}$ mesons are of the Dalitz type ($Q\bar{Q}$) or of the Jaffe type ($Q^2\bar{Q}^2$) is not yet decided. In the coupling to the baryons, we assume here that the basic process is described by the QPC model [8]. It has been shown in part I that this seems rather successful, justifying this assumption.

With a combined treatment of the NN and YN channels we aim at a high-quality description of the baryon-baryon interactions. By high quality we understand here a YN fit with low χ^2 such that, while keeping the constraints forced on the potentials by the NN fit, the free parameters with a clear physical significance, like, e.g., the $F/(F + D)$ ratios α_{PV} and α_V^m assume realistic values.

Such a combined study of all baryon-baryon interactions, and especially NN and YN , is desirable if one wants:

- (i) To study the assumption of broken SU(3) symmetry. For example we want to investigate the properties of the scalar mesons [$\varepsilon(760)$, $f_0(975)$, $a_0(980)$, $\kappa(1000)$]. We note that especially the status of the scalar nonet is at present not established yet.
- (ii) To determine $F/(F + D)$ ratios.
- (iii) To extract, in spite of the scarce experimental YN data, information about scattering lengths, effective ranges, the existence of resonances, etc.
- (iv) To provide realistic baryon-baryon potentials, which can be applied in few-body computations, nuclear and hyperonic matter studies.
- (v) To extend the theoretical description to the $\Lambda\Lambda$ and ΞN channels, where experiments may be realized in the foreseeable future.

In the construction of the ESC models there are two important options:

- (i) First, there is the choice of PV or PS coupling for the pseudoscalar mesons, or some mixture, regulated by the a_{PV} parameter, of these. This choice affects some $1/M^2$ terms in the PS-PS exchange potentials.
- (ii) Second, medium-strong symmetry breaking of the couplings, regulated by a Δ_{FSB} parameter.

We have accordingly produced four different solutions, fitting simultaneously the $NN \oplus YN$ data, which are referred to as follows: ESC04a($\Delta_{FSB} \neq 0$, $a_{PV} = 0.5$), ESC04b($\Delta_{FSB} \neq 0$, $a_{PV} = 1.0$), ESC04c($\Delta_{FSB} = 0$, $a_{PV} = 0.5$), ESC04d($\Delta_{FSB} = 0$, $a_{PV} = 1.0$). Here, $a_{PV} = 1.0$ and $a_{PV} = 0.0$ means pure pseudovector respectively purely pseudoscalar coupling. It appears that there are notable differences

between these models, in particularly their properties for matter, e.g., well-depths U_Λ , U_Σ , and U_Ξ , are rather distinct.

We will display and discuss in this article only the results for the ESC04a model in detail. With the exception of the G -matrix results, we will be very brief on ESC04b–d and will compare these models only very globally. So, in the following, by ESC04 is meant ESC04a, unless specified otherwise.

As in all Nijmegen models, the Coulomb interaction is included exactly, for which we solve the multichannel Schrödinger equation on the physical particle basis. The nuclear potentials are calculated on the isospin basis to limit the number of different form factors. This means that we include only the so-called medium-strong SU(3) breaking in the potentials.

The contents of this article are as follows. In Sec. II we describe the $S = -1$ YN channels on the isospin and particle basis, and the use of the multichannel Schrödinger equation is mentioned. The potentials in momentum and configuration space are defined by referring to the description given in part I. The BBM couplings are discussed both in the 3×3 matrix and the Cartesian octet representation. The SU(3) couplings of the OBE and TME graphs are given in a form suitable for a digital evaluation.

In Sec. III the meson-pair interaction Hamiltonians are given in the context of SU(3). Expressions for the MPE graphs are given, again in an immediately programmable form. In Sec. IV the medium-strong breaking of SU(3) symmetry of the coupling constants is described. The QPC model is employed for the development of a universal scheme for this breaking. Here also the detailed prescription for the handling of the cutoff parameters is given, in particularly for the cases of meson mixing.

In Sec. V the simultaneous $NN \oplus YN$ fitting procedure is reviewed. In Sec. VI the results for the coupling constants and $F/(F + D)$ ratios for OBE and MPE are given. They are discussed and compared with the predictions of the QPC model. Here, also the values of the BBM couplings are displayed for pseudoscalar, vector, scalar, and axial-vector mesons. In Sec. VII the NN results from the combined $NN \oplus YN$ fit, model ESC04a, henceforth called ESC04, are discussed and compared with the results of part I, referred to ESC04(NN). In Sec. VIII we discuss the fit to the YN -scattering

data from the combined $NN \oplus YN$ fit. In Sec. IX we compare very briefly the models ESC04a–d.

In Sec. X, the hypernuclear properties of ESC04a–d are studied through the G -matrix calculations for YN (ΛN , ΣN , ΞN) and their partial-wave contributions. Here, the implications of possible three-body effects for the nuclear saturation and baryon well-depths are discussed. Also, the $\Lambda\Lambda$ interactions in ESC04a–d are demonstrated to be consistent with the observed data of ${}^6_{\Lambda\Lambda}\text{He}$. In Sec. XI we finish by a final discussion and draw some conclusions.

II. CHANNELS, POTENTIALS, AND SU(3) SYMMETRY

A. Channels and potentials

In this article we consider the hyperon-nucleon reactions with $S = -1$

$$Y(p_a, s_a) + N(p_b, s_b) \rightarrow Y(p'_a, s'_a) + N(p'_b, s'_b). \quad (1)$$

Like in Refs. [3,4] we also refer to Y and Y' as particles 1 and 3 and to N and N' as particles 2 and 4. For the kinematics and the definition of the amplitudes, we refer to part I [1] of this series. Similar material can be found in Ref. [3]. Also, in part I the derivation of the Lippmann-Schwinger equation in the context of the relativistic two-body equation is described.

On the physical particle basis, there are four charge channels:

$$\begin{aligned} q = +2 &: \Sigma^+ p \rightarrow \Sigma^+ p, \\ q = +1 &: (\Lambda p, \Sigma^+ n, \Sigma^0 p) \rightarrow (\Lambda p, \Sigma^+ n, \Sigma^0 p), \\ q = 0 &: (\Lambda n, \Sigma^0 n, \Sigma^- p) \rightarrow (\Lambda n, \Sigma^0 n, \Sigma^- p), \\ q = -1 &: \Sigma^- n \rightarrow \Sigma^- n. \end{aligned} \quad (2)$$

Like in Refs. [3,4], the potentials are calculated on an isospin basis. For $S = -1$ hyperon-nucleon systems there are only two isospin channels: (i) $I = \frac{1}{2}$: (ΛN , $\Sigma N \rightarrow \Lambda N$, ΣN) and (ii) $I = \frac{3}{2}$: $\Sigma N \rightarrow \Sigma N$.

Obviously, the potential on the particle basis for the $q = 2$ and $q = -1$ channels are given by the $I = \frac{3}{2}$ ΣN potential on the isospin basis. For $q = 1$ and $q = 0$, the potentials are related to the potentials on the isospin basis by an isospin rotation. Using a notation where we only list the hyperons [$V_{\Lambda\Sigma^+} = (\Lambda p|V|\Sigma^+ n)$, etc.], we find for $q = 1$

$$\begin{pmatrix} V_{\Lambda\Lambda} & V_{\Lambda\Sigma^+} & V_{\Lambda\Sigma^0} \\ V_{\Sigma^+\Lambda} & V_{\Sigma^+\Sigma^+} & V_{\Sigma^+\Sigma^0} \\ V_{\Sigma^0\Lambda} & V_{\Sigma^0\Sigma^+} & V_{\Sigma^0\Sigma^0} \end{pmatrix} = \begin{pmatrix} V_{\Lambda\Lambda} & \sqrt{\frac{2}{3}}V_{\Lambda\Sigma} & -\sqrt{\frac{1}{3}}V_{\Lambda\Sigma} \\ \sqrt{\frac{2}{3}}V_{\Sigma\Lambda} & \frac{2}{3}V_{\Sigma\Sigma}(\frac{1}{2}) + \frac{1}{3}V_{\Sigma\Sigma}(\frac{3}{2}) & \frac{1}{3}\sqrt{2}[V_{\Sigma\Sigma}(\frac{3}{2}) - V_{\Sigma\Sigma}(\frac{1}{2})] \\ -\sqrt{\frac{1}{3}}V_{\Sigma\Lambda} & \frac{1}{3}\sqrt{2}[V_{\Sigma\Sigma}(\frac{3}{2}) - V_{\Sigma\Sigma}(\frac{1}{2})] & \frac{1}{3}V_{\Sigma\Sigma}(\frac{1}{2}) + \frac{2}{3}V_{\Sigma\Sigma}(\frac{3}{2}) \end{pmatrix}, \quad (3)$$

whereas for $q = 0$ we find

$$\begin{pmatrix} V_{\Lambda\Lambda} & V_{\Lambda\Sigma^0} & V_{\Lambda\Sigma^-} \\ V_{\Sigma^0\Lambda} & V_{\Sigma^0\Sigma^0} & V_{\Sigma^0\Sigma^-} \\ V_{\Sigma^-\Lambda} & V_{\Sigma^-\Sigma^0} & V_{\Sigma^-\Sigma^-} \end{pmatrix} = \begin{pmatrix} V_{\Lambda\Lambda} & \sqrt{\frac{1}{3}}V_{\Lambda\Sigma} & -\sqrt{\frac{2}{3}}V_{\Lambda\Sigma} \\ \sqrt{\frac{1}{3}}V_{\Sigma\Lambda} & \frac{1}{3}V_{\Sigma\Sigma}(\frac{1}{2}) + \frac{2}{3}V_{\Sigma\Sigma}(\frac{3}{2}) & \frac{1}{3}\sqrt{2}[V_{\Sigma\Sigma}(\frac{3}{2}) - V_{\Sigma\Sigma}(\frac{1}{2})] \\ -\sqrt{\frac{2}{3}}V_{\Sigma\Lambda} & \frac{1}{3}\sqrt{2}[V_{\Sigma\Sigma}(\frac{3}{2}) - V_{\Sigma\Sigma}(\frac{1}{2})] & \frac{2}{3}V_{\Sigma\Sigma}(\frac{1}{2}) + \frac{1}{3}V_{\Sigma\Sigma}(\frac{3}{2}) \end{pmatrix}. \quad (4)$$

For the kinematics of the reactions and the various thresholds; see Ref. [4]. In this work we do not solve the Lippmann-Schwinger equation, but the multichannel Schrödinger equation in configuration space, completely analogous to Ref. [3]. The multichannel Schrödinger equation for the configuration-space potential is derived from the Lippmann-Schwinger equation through the standard Fourier transform, and the equation for the radial wave function is found to be of the form [3]

$$u''_{l,j} + (p_i^2 \delta_{i,j} - A_{i,j})u_{l,j} - B_{i,j}u'_{l,j} = 0, \quad (5)$$

where $A_{i,j}$ contains the potential, nonlocal contributions, and the centrifugal barrier, whereas $B_{i,j}$ is present only when nonlocal contributions are included. The solution in the presence of open and closed channels is given, for example, in Ref. [13]. The inclusion of the Coulomb interaction in the configuration-space equation is well known and included in the evaluation of the scattering matrix.

The momentum space and configuration space potentials for the ESC04 model have been described in part I [1] for baryon-baryon in general. Therefore, they apply also to hyperon-nucleon and we can refer for that part of the potential to part I. Also in the ESC model, the potentials are of such a form that they are exactly equivalent in both momentum space and configuration space. The treatment of the mass differences among the baryons are handled exactly similar as is done in Refs. [3,4]. Also, exchange potentials related to strange meson exchange K , K^* etc., can be found in these references.

The baryon mass differences in the intermediate states for TME and MPE potentials has been neglected for YN scattering. This, although possible in principle, becomes rather laborious and is not expected to change the characteristics of the baryon-baryon potentials much.

B. BBM couplings in SU(3) and matrix representations

In previous work of the Nijmegen group, e.g., Refs. [3] and [4], the treatment of SU(3) has been given in detail for the BBM interaction Lagrangians and the coupling coefficients of the OBE graphs. However, for the ESC models we also need the coupling coefficients for the TME and the MPE graphs. Because there are many more TME and MPE graphs than OBE graphs, a computerized computation is desirable. For that purpose we found the so-called Cartesian octet representation quite useful. Therefore, we give an exposition of this representation, its connection with the matrix representation used in our previous work, and the formulation of the coupling coefficients used in the automatic computation.

In the matrix representation, the eight $J^P = \frac{1}{2}^+$ baryons are described by a traceless matrix, see, e.g., Ref. [14],

$$B = \begin{pmatrix} \frac{\Sigma^0}{\sqrt{2}} + \frac{\Lambda}{\sqrt{6}} & & \Sigma^+ & p \\ & \Sigma^- & -\frac{\Sigma^0}{\sqrt{2}} + \frac{\Lambda}{\sqrt{6}} & n \\ & & & & -\frac{2\Lambda}{\sqrt{6}} \\ -\Xi^- & & \Xi^0 & & \end{pmatrix}. \quad (6)$$

Similarly, the various meson nonets (we take the pseudoscalar mesons with $J^P = 0^+$ as an example) are represented by

$$P = P_{\{1\}} + P_{\{8\}}, \quad (7)$$

where the singlet matrix $P_{\{1\}}$ has elements $\eta_0/\sqrt{3}$ on the diagonal and the octet matrix $P_{\{8\}}$ is given by

$$P_{\{8\}} = \begin{pmatrix} \frac{\pi^0}{\sqrt{2}} + \frac{\eta_8}{\sqrt{6}} & & \pi^+ & & K^+ \\ & \pi^- & & -\frac{\pi^0}{\sqrt{2}} + \frac{\eta_8}{\sqrt{6}} & & K^0 \\ & & K^- & & \bar{K}^0 & -\frac{2\eta_8}{\sqrt{6}} \end{pmatrix}. \quad (8)$$

Exploiting the SU(3)-invariant combinations, see, e.g., Refs. [4,14], $[\bar{\text{B}}\text{B}P]_F$, $[\bar{\text{B}}\text{B}P]_D$, and $[\bar{\text{B}}\text{B}P]_S$, the SU(3)-invariant BBP-interaction Lagrangian can be written as [14]

$$\mathcal{L}_I = -g_8 \sqrt{2} [\alpha [\bar{\text{B}}\text{B}P]_F + (1 - \alpha) [\bar{\text{B}}\text{B}P]_D] - g_1 \sqrt{\frac{1}{3}} [\bar{\text{B}}\text{B}P]_S, \quad (9)$$

where g_8 and g_1 are the singlet and octet couplings, α is known as the $F/(F+D)$ ratio, and the square-root factors are introduced for later convenience.

The convention used for the isospin doublets is

$$N = \begin{pmatrix} p \\ n \end{pmatrix}, \quad \Xi = \begin{pmatrix} \Xi^0 \\ \Xi^- \end{pmatrix}, \\ K = \begin{pmatrix} K^+ \\ K^0 \end{pmatrix}, \quad K_c = \begin{pmatrix} \bar{K}^0 \\ -K^- \end{pmatrix}, \quad (10)$$

and for the isovectors in the $\text{SU}(2)_I$ tensor notation ($a, b = 1, 2$)

$$\pi_b^a = \begin{pmatrix} \frac{\pi^0}{\sqrt{2}} & \pi^+ \\ \pi^- & -\frac{\pi^0}{\sqrt{2}} \end{pmatrix}, \quad \Sigma_b^a = \begin{pmatrix} \frac{\Sigma^0}{\sqrt{2}} & \Sigma^+ \\ \Sigma^- & -\frac{\Sigma^0}{\sqrt{2}} \end{pmatrix} \quad (11)$$

where we have chosen the phases of the isovector fields such [14] that

$$\Sigma \cdot \pi = \sum_{a,b=1}^3 \Sigma_b^a \pi_a^b = \Sigma^+ \pi^- + \Sigma^0 \pi^0 + \Sigma^- \pi^+. \quad (12)$$

The expression of the interaction Lagrangian (9) in terms of the isospin singlets ($I = 0$), doublets ($I = 1/2$), and triplets ($I = 1$), is given, e.g., in Ref. [4]. Also, the BBM couplings of the octet members are given in terms of g_8 and $\alpha = F/(F+D)$. See Ref. [4], Eqs. (2.10)–(2.14).

C. Cartesian octet representation

The annihilation operators corresponding to the baryon and pseudoscalar SU(3) octet representation {8} are given in Table I. Here we used the Cartesian octet fields. For baryons these are denoted by ψ_i ($i = 1, 2, \dots, 8$), and for the pseudoscalar mesons by ϕ_i ($i = 1, 2, \dots, 8$) [14–16]. The particle states are created by these operators are given in Table II [14].

TABLE I. Octet representation baryons and mesons.

$\Sigma^+ = \frac{1}{\sqrt{2}}(\psi_1 - i\psi_2)$	$\pi^+ = \frac{1}{\sqrt{2}}(\phi_1 - i\phi_2)$
$\Sigma^- = \frac{1}{\sqrt{2}}(\psi_1 + i\psi_2)$	$\pi^- = \frac{1}{\sqrt{2}}(\phi_1 + i\phi_2)$
$\Sigma^0 = \psi_3$	$\pi^0 = \phi_3$
$p = \frac{1}{\sqrt{2}}(\psi_4 - i\psi_5)$	$K^+ = \frac{1}{\sqrt{2}}(\phi_4 - i\phi_5)$
$n = \frac{1}{\sqrt{2}}(\psi_6 - i\psi_7)$	$K^0 = \frac{1}{\sqrt{2}}(\phi_6 - i\phi_7)$
$\Xi^- = \frac{1}{\sqrt{2}}(\psi_4 + i\psi_5)$	$K^- = \frac{1}{\sqrt{2}}(\phi_4 + i\phi_5)$
$\Xi^0 = \frac{1}{\sqrt{2}}(\psi_6 + i\psi_7)$	$\bar{K}^0 = \frac{1}{\sqrt{2}}(\phi_6 + i\phi_7)$
$\Lambda = \psi_8$	$\eta = \phi_8$

Similar expressions hold for the vector, axial-vector, and scalar mesons. The connection between the matrix representation (6) and the Cartesian octet representation is

$$B_b^a = \frac{1}{\sqrt{2}} \sum_{i=1}^8 (\lambda_i)_{ab} \psi_i, \quad \psi_i = \frac{1}{\sqrt{2}} \sum_{a,b=1}^3 (\lambda_i)_{ab} B_b^a, \quad (13)$$

where λ_i , $i = 1, 8$ are the Gell-Mann matrices [14], and where the indices $(a, b = 1, 2, 3)$. The same expression holds for P_b^a of (8) in terms of the ϕ_i s. The SU(3) invariants in the Cartesian octet representation read

$$[\bar{B}B]_F = \sum_{i,j,k=1}^8 f_{ijk} [\bar{\psi}_i \psi_j] \phi_k, \quad (14a)$$

$$[\bar{B}B]_D = \sum_{i,j,k=1}^8 d_{ijk} [\bar{\psi}_i \psi_j] \phi_k, \quad (14b)$$

$$[\bar{B}B]_S = \sum_{i,j=1}^8 \delta_{ji} [\bar{\psi}_i \psi_j] \phi_9, \quad (14c)$$

where f_{ijk} are the totally antisymmetric SU(3) structure constants, d_{ijk} are the totally symmetric constants, and ϕ_9 denotes the unitary singlet. They are given by the following commutators and anticommutators

$$[\lambda_i, \lambda_j] = 2if_{ijk}\lambda_k, \quad \{\lambda_i, \lambda_j\} = \frac{4}{3}\delta_{ij} + 2d_{ijk}\lambda_k. \quad (15)$$

The baryon-baryon matrix elements can now be computed using the Cartesian octet states

$$\langle B_3, B_4 | M | B_1, B_2 \rangle = C_{3j}^* C_{4n}^* M(j, n; i, m) C_{1i} C_{2m}, \quad (16)$$

where C coefficients relate the particle states to the Cartesian states, see Table II, and $M(j, n; i, m)$ depends on the structure

TABLE II. Octet particle states.

$ \pi^+\rangle = -\pi^{\dagger} 0\rangle$	$ \Sigma^+\rangle = -\Sigma^{\dagger} 0\rangle$
$ \pi^-\rangle = \pi^{-\dagger} 0\rangle$	$ \Sigma^-\rangle = \Sigma^{-\dagger} 0\rangle$
$ \pi^0\rangle = \pi^{0\dagger} 0\rangle$	$ \Sigma^0\rangle = \Sigma^{0\dagger} 0\rangle$
$ K^+\rangle = K^{+\dagger} 0\rangle$	$ p\rangle = p^{\dagger} 0\rangle$
$ K^0\rangle = K^{0\dagger} 0\rangle$	$ n\rangle = n^{\dagger} 0\rangle$
$ K^-\rangle = K^{-\dagger} 0\rangle$	$ \Xi^-\rangle = \Xi^{-\dagger} 0\rangle$
$ \bar{K}^0\rangle = \bar{K}^{0\dagger} 0\rangle$	$ \Xi^0\rangle = \Xi^{0\dagger} 0\rangle$
$ \eta_8\rangle = \eta_8^{\dagger} 0\rangle$	$ \Lambda\rangle = \Lambda^{\dagger} 0\rangle$

of the graph. Below, we work out the M operator for OBE, TME, and MPE graphs in the Cartesian octet representation. Then, the physical two-baryon matrix elements in (16) can be obtained easily.

D. Computations for OBE and TME SU(3) factors

1. One-boson exchange

The SU(3) matrix element for the OBE graph in Fig. 1 is given by

$$M_{\text{obe}}(j, n; i, m) = \sum_p^i H_1^{(a)}(j, i, p) H_2^{(a)}(n, m, p), \quad (17)$$

where $a = P, V, A, S$ and

$$H_a(j, i, p) = [2g_8^{(a)}\{i\alpha f_{jip} + (1 - \alpha)d_{jip}\} + g_1^{(a)}\delta_{ji}\delta_{p9}], \quad (18)$$

The summation over p determines which mesons contribute to (18), and the prime indicates that one may restrict this summation to pick out a particular meson. This is in general necessary because within an SU(3) nonet the mesons have different masses, and we need their couplings separately for a proper calculation of the potentials.

To illustrate this method of computation we consider π exchange in $\Sigma N \rightarrow \Sigma N$. We have

$$\begin{aligned} \langle \Sigma^+ n | M_{\pi} | \Sigma^+ n \rangle &= \frac{1}{4} \sum_{i,j,m,n=1}^8 \sum_{p=1}^3 \langle \psi_1 - i\psi_2 | \psi_j \rangle \cdot \\ &\quad \times \langle \psi_6 - i\psi_7 | \psi_n \rangle \langle \psi_j \psi_n | M_{\pi} | \psi_i \psi_m \rangle \cdot \\ &\quad \times \langle \psi_i | \psi_1 - i\psi_2 \rangle \langle \psi_m | \psi_6 - i\psi_7 \rangle \\ &= \frac{1}{4} \sum_{i,j,m,n=1}^8 \sum_{p=1}^3 (\delta_{1j} + i\delta_{2j})(\delta_{6n} + i\delta_{7n}) \cdot \\ &\quad \times (\delta_{1i} - i\delta_{2i})(\delta_{6n} - i\delta_{7n}) \langle \psi_j \psi_n | M_{\pi} | \psi_i \psi_m \rangle \\ &= \frac{1}{4} \sum_{i,j=1}^2 \sum_{m,n=6}^7 \sum_{p=1}^3 Z(j, i) Z(n - j, m - i) \cdot \\ &\quad \times \{g_8^{(P)}[-i\alpha_{PV} f_{jip} + (1 - \alpha_{PV})d_{jip}] + g_1^{(P)}\delta_{ji}\delta_{p8}\} \cdot \\ &\quad \times \{g_8^{(P)}[-i\alpha_{PV} f_{nmp} + (1 - \alpha_{PV})d_{nmp}] + g_1^{(P)}\delta_{nm}\delta_{p8}\}, \end{aligned} \quad (19)$$

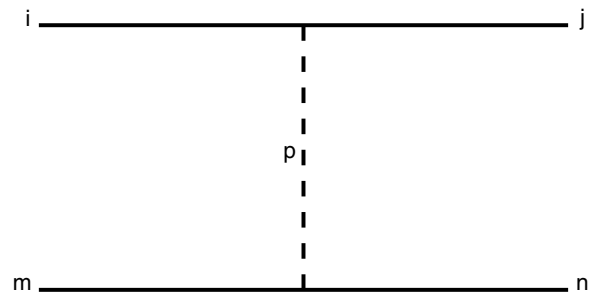


FIG. 1. Octet representation indices OBE graphs. The solid lines denote baryons with labels i, m, j, n . The dashed line with label p refers to the bosons: pseudoscalar, vector, axial-vector, or scalar mesons.

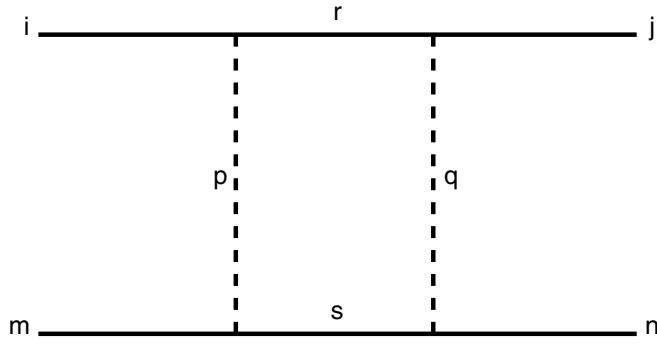


FIG. 2. Octet representation indices TME parallel graphs. The solid lines denote baryons with labels i, m, j, n, r, s . The dashed lines with labels p, q refer to the pseudoscalar mesons.

where the 2×2 matrix Z is defined as

$$Z = \begin{pmatrix} 1 & -i \\ i & 1 \end{pmatrix}. \quad (20)$$

2. Two-meson exchange

The SU(3) matrix elements for the parallel (//) and crossed (X) TME-graphs in Figs. 2 and 3 are given by

$$M_{\text{tme}}^{(//)}(j, n; i, m) = \sum_{p,q,r,s} H_2(j, r, q) H_1(r, i, p) \times H_2(n, s, q) H_1(s, m, p) \quad (21)$$

$$M_{\text{tme}}^{(X)}(j, n; i, m) = \sum_{p,q,r,s} H_2(j, r, q) H_1(r, i, p) \times H_1(n, s, q) H_2(s, m, p) \quad (22)$$

Again, like in the OBE case, the numerical values of the SU(3) matrix elements for TME can be computed easily making a computer program.

III. MPE INTERACTIONS AND SU(3)

A. Pair couplings and SU(3) symmetry

Below, $\sigma, \mathbf{a}_0, \mathbf{A}_1, \dots$ are shorthand for, respectively, the nucleon densities $\bar{\psi}\psi, \bar{\psi}\boldsymbol{\tau}\psi, \bar{\psi}\gamma_5\boldsymbol{\gamma}_\mu\boldsymbol{\tau}\psi, \dots$

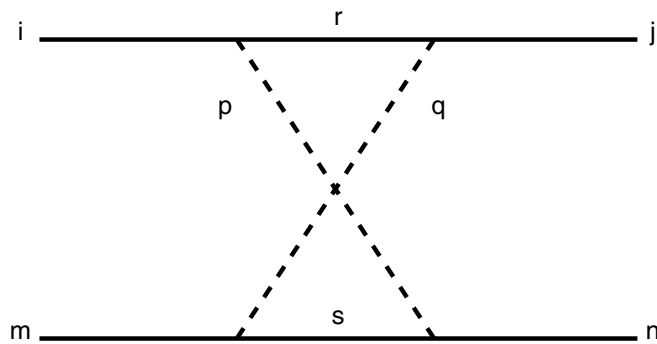


FIG. 3. Octet representation indices TME crossed graphs. The solid lines denote baryons with labels i, m, j, n, r, s . The dashed lines with labels p and q refer to the pseudoscalar mesons.

The SU(3) octet and singlet mesons, denoted by the subscripts 8 and 1, respectively, are in terms of the physical ones defined as follows:

1. Pseudoscalar mesons

$$\begin{aligned} \eta_1 &= \cos \theta_{PV} \eta' - \sin \theta_{PV} \eta \\ \eta_8 &= \sin \theta_{PV} \eta' + \cos \theta_{PV} \eta \end{aligned}$$

Here, η' and η are the physical pseudoscalar mesons $\eta(957)$ respectively $\eta(548)$.

2. Vector mesons

$$\begin{aligned} \phi_1 &= \cos \theta_V \omega - \sin \theta_V \phi \\ \phi_8 &= \sin \theta_V \omega + \cos \theta_V \phi \end{aligned}$$

Here, ϕ and ω are the physical vector mesons $\phi(1019)$ respectively $\omega(783)$.

Then, one has the following SU(3)-invariant pair-interaction Hamiltonians:

(i) SU(3) singlet couplings $S_\beta^\alpha = \delta_\beta^\alpha \sigma / \sqrt{3}$:

$$\mathcal{H}_{S_1 P P} = \frac{g_{S_1 P P}}{\sqrt{3}} \{ \boldsymbol{\pi} \cdot \boldsymbol{\pi} + 2K^\dagger K + \eta_8 \eta_8 \} \cdot \sigma$$

(ii) SU(3) octet symmetric couplings I, $S_\beta^\alpha = (S_8)_\beta^\alpha \Rightarrow (1/4)\text{Tr}\{S[P, P]_+\}$:

$$\begin{aligned} \mathcal{H}_{S_8 P P} &= \frac{g_{S_8 P P}}{\sqrt{6}} \left\{ (\mathbf{a}_0 \cdot \boldsymbol{\pi}) \eta_8 + \frac{\sqrt{3}}{2} \mathbf{a}_0 \cdot (K^\dagger \boldsymbol{\tau} K) \right. \\ &\quad + \frac{\sqrt{3}}{2} \{ (K_0^\dagger \boldsymbol{\tau} K) \cdot \boldsymbol{\pi} + \text{h.c.} \} - \frac{1}{2} \{ (K_0^\dagger K) \eta_8 + \text{h.c.} \} \\ &\quad \left. + \frac{1}{2} f_0 (\boldsymbol{\pi} \cdot \boldsymbol{\pi} - K^\dagger K - \eta_8 \eta_8) \right\} \end{aligned}$$

(iii) SU(3) octet symmetric couplings II, $S_\beta^\alpha = (B_8)_\beta^\alpha \Rightarrow (1/4)\text{Tr}\{B^\mu[V_\mu, P]_+\}$:

$$\begin{aligned} \mathcal{H}_{B_8 V P} &= \frac{g_{B_8 V P}}{\sqrt{6}} \left\{ \frac{1}{2} [(\mathbf{B}_1^\mu \cdot \boldsymbol{\rho}_\mu) \eta_8 + (\mathbf{B}_1^\mu \cdot \boldsymbol{\pi}_\mu) \phi_8] \right. \\ &\quad + \frac{\sqrt{3}}{4} [\mathbf{B}_1 \cdot (K^{*\dagger} \boldsymbol{\tau} K) + \text{h.c.}] \\ &\quad + \frac{\sqrt{3}}{4} [(K_1^\dagger \boldsymbol{\tau} K^*) \cdot \boldsymbol{\pi} + (K_1^\dagger \boldsymbol{\tau} K) \cdot \boldsymbol{\rho} + \text{h.c.}] \\ &\quad - \frac{1}{4} [(K_1^\dagger \cdot K^*) \eta_8 + (K_1^\dagger \cdot K) \phi_8 + \text{h.c.}] \\ &\quad \left. + \frac{1}{2} H^0 \left[\boldsymbol{\rho} \cdot \boldsymbol{\pi} - \frac{1}{2} (K^{*\dagger} \cdot K + \text{h.c.}) - \phi_8 \eta_8 \right] \right\} \end{aligned}$$

(iv) SU(3) octet a-symmetric couplings I, $A_\beta^\alpha = (V_8)_\beta^\alpha \Rightarrow (-i/\sqrt{2})\text{Tr}\{V^\mu[P, \partial_\mu P]_-\}$:

$$\begin{aligned} \mathcal{H}_{V_8 P P} &= g_{A_8 P P} \left\{ \frac{1}{2} \boldsymbol{\rho}_\mu \cdot \boldsymbol{\pi} \times \hat{\partial}^\mu \boldsymbol{\pi} + \frac{i}{2} \boldsymbol{\rho}_\mu \cdot (K^\dagger \boldsymbol{\tau} \hat{\partial}^\mu K) \right. \\ &\quad + \frac{i}{2} \left[K_\mu^{*\dagger} \boldsymbol{\tau} (K \hat{\partial}^\mu \boldsymbol{\pi}) - \text{h.c.} \right] + i \frac{\sqrt{3}}{2} \\ &\quad \left. \times [K_\mu^{*\dagger} \cdot (K \cdot \hat{\partial}^\mu \eta_8) - \text{h.c.}] + \frac{i}{2} \sqrt{3} \phi_\mu (K^\dagger \hat{\partial}^\mu K) \right\} \end{aligned}$$

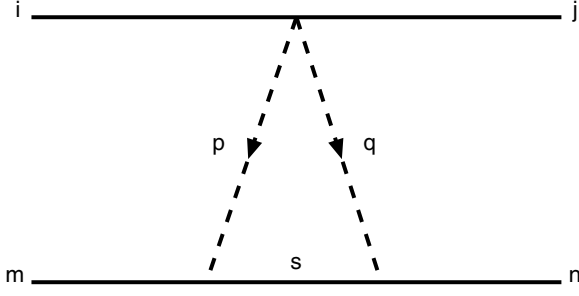


FIG. 4. Octet representation indices MPE one-pair graphs. The solid lines denote baryons with labels i, m, j, n, s . The dashed lines with labels p and q refer to the pseudoscalar, etc., mesons.

(v) SU(3) octet asymmetric couplings II, $A_\beta^\alpha = (A_8)_{\beta}^\alpha \Rightarrow (-i/\sqrt{2})\text{Tr}\{A^\mu[P, V_\mu]_-\}$:

$$\begin{aligned} \mathcal{H}_{A_8VP} = g_{A_8VP} & \left\{ \mathbf{A}_1 \cdot \boldsymbol{\pi} \times \boldsymbol{\rho} \right. \\ & + \frac{i}{2} \mathbf{A}_1 \cdot [(K^\dagger \boldsymbol{\tau} K^*) - (K^{*\dagger} \boldsymbol{\tau} K)] \\ & - \frac{i}{2} [((K^\dagger \boldsymbol{\tau} K_A) \cdot \boldsymbol{\rho} + (K_A^\dagger \boldsymbol{\tau} K^*) \cdot \boldsymbol{\pi}) - \text{h.c.}] \\ & - i \frac{\sqrt{3}}{2} [((K^\dagger \cdot K_A) \phi_8 + (K_A^\dagger \cdot K^*) \eta_8) - \text{h.c.}] \\ & \left. + \frac{i}{2} \sqrt{3} f_1 [K^\dagger \cdot K^* - K^{*\dagger} \cdot K] \right\} \end{aligned}$$

The relation with the pair couplings of Ref. [17] and part I is $g_{S_1PP}/\sqrt{3} = g_{(\pi\pi)_0}/m_\pi$, $g_{A_8VP} = g_{(\pi\rho)_1}/m_\pi$, etc.

B. Computations of MPE SU(3) factors

The SU(3) matrix elements for the graphs with meson-pair vertices, the so-called MPE graphs (Figs. 4 and 5) are, using the Cartesian octet representation in Sec. II C, given by

$$\begin{aligned} M_{(1\text{-pair})}(j, n; i, m) = \sum_{p,q,r,s}^I & H_{\text{pair}}(j, i, s) O(q, p, s) \\ & \times H_2(m, r, q) H_1(r, m, p) \end{aligned} \quad (23)$$

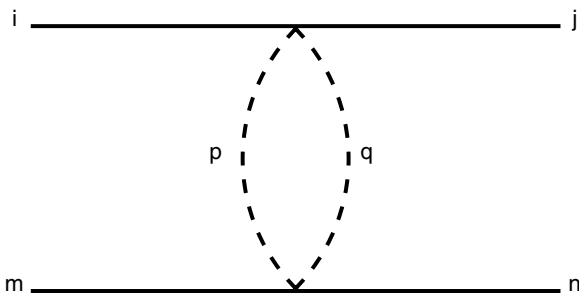


FIG. 5. Octet representation indices MPE two-pair graphs. The solid lines denote baryons with labels i, m, j, n . The dashed lines with labels p and q refer to the pseudoscalar, etc., mesons.

$$\begin{aligned} M_{(2\text{-pair})}(j, n; i, m) = \sum_{p,q,r,s=1}^I & H_{\text{pair}}(j, i, s) O(q, p, s) \\ & \times O(q, p, r) H_{\text{pair}}(n, m, p), \end{aligned} \quad (24)$$

Again, like in the OBE case, the numerical values of the SU(3) matrix elements for MPE can be computed straightforwardly by use of a computer program.

IV. BROKEN SU(3) COUPLINGS AND FORM FACTORS

A. Broken SU(3) BBM couplings

In our models, breaking of the SU(3) symmetry is introduced in several places. First of all, we use the physical masses for the baryons and mesons. Second, we allow for the fact that the Λ and Σ^0 have the same quark content, and so there is an appreciable mixing between the isospin-pure Λ and Σ^0 states [12]. Although exact $SU(2) \subset SU(3)$ symmetry requires that $f_{\Lambda\Lambda\pi^0} = 0$, Λ - Σ^0 mixing and the interaction $\Sigma^0 \rightarrow \Lambda + \pi^0$ result in a nonzero coupling constant for the physical Λ -hyperon, derived by Dalitz and von Hippel [12]. This Λ - Σ^0 mixing leads also to a nonzero coupling of the Λ to the other $I = 1$ mesons: $\rho(760)$, $a_0(980)$, $a_1(1270)$, as well as to the $I = 1$ pairs. For the details of these OBE couplings see, e.g., Ref. [4], Eqs. (15)–(17). The corresponding so-called CSB potentials are included in the ESC model for OBE, TME, and MPE.

In paper I of this series we have shown that the NNM coupling constants are described pretty well by the 3P_0 mechanism [8,18,19]. In this article we use the predictions of the 3P_0 model for the $F/(F+D)$ ratios as well. Therefore, it is most natural to use for the description of a possible flavor symmetry breaking of the coupling constants the 3P_0 mechanism as well, like in Ref. [4]. In Ref. [4] it is argued that a symmetric treatment of the “moving” quarks and the pair quarks in the 3P_0 -coupling process is appropriate, because this leads to a covariant vertex. Therefore, in Ref. [4] the 3P_0 Hamiltonian for the BBM couplings is taken as follows

$$\begin{aligned} H_I = \int d^3x \int d^3y & F(x-y) \cdot \\ & \times [\bar{q}(x) O_{\bar{q}q} q(x)]^{(1)} \otimes [\bar{q}(y) O_{\bar{q}q} q(y)]^{(2)}, \end{aligned} \quad (25)$$

where the quark-field operators are vectors in flavor space, with components $q_i = (u, d, s)$ and $\bar{q}_i = (\bar{u}, \bar{d}, \bar{s})$. (In the following we refer to the nonstrange quarks u and d as n quarks.) It is understood in Eq. (25) that the first factor creates or annihilates a quark pair, whereas the second factor “moves” a quark from the baryon into the meson or vice versa. O is a matrix in quark-flavor space, which, supposing no quark mixing, is diagonal. However, because it will in general break SU(3) and SU(2) symmetry by using the form

$$(O_{\bar{q}q})_{i,j} = \begin{pmatrix} \gamma_u & 0 & 0 \\ 0 & \gamma_d & 0 \\ 0 & 0 & \gamma_s \end{pmatrix}, \quad (26)$$

where the pair-creation constants γ_u , γ_d , and γ_s in principle could be unequal. The CSB described above is on the quark-level because of $\gamma_u \neq \gamma_d$. For a more detailed description of

some properties of the Hamiltonian in (25) and $(O_{\bar{q}q})_{i,j}$ we refer to Ref. [4].

Here, we assume that there is, also flavor-symmetry breaking (FSB) of the medium-strong kind, i.e., $\gamma_n = \gamma_u = \gamma_d \neq \gamma_s$. We introduce this medium strong SU(3) breaking according to the 3P_0 model by a modification of the $s\bar{s}$ coupling, using the ratio $\Delta_{\text{FSB}} = \gamma_s/\gamma_n - 1$. For $\Delta_{\text{FSB}} = 0$ there is no SU(3) breaking, whereas for $\Delta_{\text{FSB}} \neq 0$.

The $I = 1$ meson couplings for NN are determined in the process of NN fitting. This fixes γ_n . In the coupling of the $I = 1/2$ mesons, K , K^* , κ , only one $s\bar{s}$ operator is active and the SU(3) breaking of the coupling is given by

$$\Delta g_{\Lambda NK} = \Delta_{\text{FSB}} \hat{g}_{\Lambda NK}, \quad (27)$$

and completely similar expressions for $\Delta g_{\Sigma NK}$, $\Delta g_{\Xi \Lambda K}$, and $\Delta g_{\Xi \Sigma K}$. Here, $\hat{g}_{\Lambda NK}$, etc., are calculated as usual in terms of $g_{NN\pi}$ and the SU(3) scheme with α_{PV} . Similar formulas we used for the SU(3) breaking in the case of the vector, axial-vector, and scalar mesons.

In the case of the $I = 0$ -mesons two $s\bar{s}$ operators are active in the baryon-baryon coupling. Now, the $I = 0$ -mesons have a $n\bar{n}$ and a $s\bar{s}$ component. In our scheme only the coupling of the $s\bar{s}$ is affected by the SU(3) breaking. Therefore, it is natural to transform first to the so-called ideal $q\bar{q}$ basis, applying the SU(3) breaking, and transform back to the physical basis. This scheme is as follows:

- (i) The $I = 0$ $|n\bar{n}\rangle = |u\bar{u} + d\bar{d}\rangle/\sqrt{2}$ and the $-|s\bar{s}\rangle$ states are in SU(3) linear combinations of the {1} and {8} octet states. Likewise, the coupling of the $n\bar{n}$ and $s\bar{s}$ quark pairs to baryons are the same linear combinations, i.e.,

$$\begin{aligned} \hat{g}_{n\bar{n}} &= \cos \theta_I \hat{g}_1 + \sin \theta_I \hat{g}_8, \\ \hat{g}_{s\bar{s}} &= -\sin \theta_I \hat{g}_1 + \cos \theta_I \hat{g}_8, \end{aligned} \quad (28)$$

where $\cos \theta_I = \sqrt{2/3}$ and $\sin \theta_I = \sqrt{1/3}$.

- (ii) Because for the $s\bar{s}$ coupling process two strange quark pairs are involved, and none in the $n\bar{n}$ coupling, the FSB is given on the level of the quark-pair coupling by:

$$g_{n\bar{n}} \rightarrow \hat{g}_{n\bar{n}}, \quad g_{s\bar{s}} \rightarrow (1 + \Delta_{\text{FSB}})^2 \hat{g}_{s\bar{s}}. \quad (29)$$

- (iii) The translation of this breaking to the level of the {1} and {8} octet couplings is the inverse transformation of (29), and from there to the physical mesons. For example, in the case of the vector mesons we have

$$\begin{aligned} g_\omega &= \cos \Delta\theta_V g_1^V + \sin \Delta\theta_V g_8^V, \\ g_\phi &= -\sin \Delta\theta_V g_1^V + \cos \Delta\theta_V g_8^V, \end{aligned} \quad (30)$$

where $\Delta\theta_V = \theta_V - \theta_I$. The similar procedure is used for the pseudoscalar, scalar, and axial-vector mesons.

This breaking applies to the NNM , YNM , and YYM couplings, containing the free parameter Δ_{PS} for the pseudoscalar mesons and one parameter Δ_V , which is used for the vector, axial-vector, and scalar mesons.

We note that this breaking somewhat differs from that used in NSC97 [4], which was based on an SU(6)_W scheme. The problem with the latter, from our viewpoint is, that the states of, for example, the vector nonet are a mixture of $W = 0$ and

$W = 1$, making the implementation of SU(3) breaking less straightforward as in the scheme described above.

The implementation of this scheme in practice is done as follows. We start, for example, in the case of the vector mesons for the g couplings, with the parameter set $(\hat{g}_\rho, \hat{g}_\omega, \theta_V, \alpha_V)$ and compute all couplings in the usual SU(3) scheme, giving $\hat{g}_{NN\rho}$, $\hat{g}_{\Sigma\Sigma\rho}$, etc. This defines the singlet {1} couplings

$$\hat{g}_1 = [\hat{g}_\omega - \sin \theta_V \hat{g}_8] / \cos \theta_V$$

where the octet {8} coupling for nucleons is given by $\hat{g}_8 = (4\alpha_V - 1)\hat{g}_{NN\rho}/\sqrt{3}$ and similarly for Λ , Σ , and Ξ . Then, we compute $\hat{g}_{n\bar{n}}$ and $\hat{g}_{s\bar{s}}$ using (29). Subsequently we compute the symmetry breaking by the transformation, etc., as described above, and finally we compute the coupling constants g_ω , g_ϕ , etc.

We finish this discussion by noticing that for the $I = 1$ mesons π , ρ , a_0 , a_1 for all baryon couplings $g = \hat{g}$, because then only n quarks are ‘‘active.’’

B. Form factors

Also in this work, like in the NSC97 models [4], the form factors depend on the SU(3) assignment of the mesons. In principle, we introduce form-factor masses Λ_8 and Λ_1 for the {8} and {1} members of each meson nonet, respectively. In the application to YN and YY , we allow for SU(3) breaking, by using different cutoffs for the strange mesons K , K^* , and κ . Moreover, for the $I = 0$ -mesons we assign the cutoffs as if there were no meson mixing. For example, we assign Λ_1 for η' , ω , ϵ , and Λ_8 for η , ϕ , S^* , etc. For the axial mesons we use a single cutoff Λ^A .

V. ESC04 MODEL: FITTING $NN \oplus YN$ DATA

Like in the NN fit, described in part I, also in the simultaneous χ^2 fit of the NN and YN data, it appeared again that the OBE couplings could be constraint successfully by the ‘‘naive’’ predictions of the QPC model [18]. Although these predictions, see part I, Sec. IV, are ‘‘bare’’ ones, we tried to keep during the searches many OBE couplings rather closely in the neighborhood of the predicted values. Also, it appeared that we could either fix the $F/(F + D)$ ratios to those as suggested by the QPC model, or apply the same restraining strategy as for the OBE couplings.

In the simultaneous χ^2 fit of the NN and YN data a *single set of parameters* was used. Of course, it is to be expected that the accurate and very numerous NN data essentially fix most of the parameters. Only some of the parameters, for example, certain $F/(F + D)$ ratios, are influenced by the YN data.

A. Parameters and nucleon-nucleon fit

For the cutoff masses Λ we used as free parameters Λ_8^P , Λ_8^V , Λ_1^V , and Λ^A . The $I = 0$ cutoff masses for the pseudoscalar and scalar mesons were fixed to $\Lambda_1^P = 900$ MeV and $\Lambda_1^S \approx 1100$ MeV.

The treatment of the broad mesons ρ and ϵ is similar to that in the OBE models [3,20]. For the ρ meson the same parameters are used as in these references. However, for the $\epsilon = f_0(760)$ assuming $m_\epsilon = 760$ MeV and $\Gamma_\epsilon = 640$ MeV

the Bryan-Gersten parameters [21] are used. For the chosen mass and width they are: $m_1 = 496.39796$ MeV, $m_2 = 1365.59411$ MeV, and $\beta_1 = 0.21781$, $\beta_2 = 0.78219$. The “mass” of the diffractive exchanges were all fixed to $m_P = 309.1$ MeV.

Summarizing the parameters we have for NN :

- (i) QPC constrained: $g_{NN\rho}, g_{NN\omega}, f_{NN\rho}, f_{NN\omega}, f_{NNa_1}, g_{a_0}, g_{NN\epsilon}, g_{NNA_2}, g_{NNP},$
- (ii) Pair couplings: $g_{NN(\pi\pi)_1}, f_{NN(\pi\pi)_1}, g_{NN(\pi\rho)_1}, g_{NN\pi\omega}, g_{NN\pi\eta}, g_{NN\pi\epsilon},$
- (iii) Cutoff masses: $\Lambda_8^P, \Lambda_8^V, \Lambda_8^S, \Lambda_1^V, \Lambda^A.$

Of course, also the couplings for the pseudoscalar mesons $f_{NN\pi}, f_{NN\eta}$ were fitted. The pair coupling $g_{NN(\pi\pi)_0}$ was kept fixed at a small, but otherwise arbitrary, value.

The NN data used are the same as in part I, and we refer the reader to this article for a description of the employed phase-shift analysis [22,23]. Differences with part I are that here we did not fit the NN low-energy parameters and the deuteron binding energy explicitly.

B. Parameters and hyperon-nucleon fit

All “best” low-energy YN data are included in the fitting. This is a selected set of 35 low-energy YN data, the same set has been used in Refs. [3] and [4]. We added three (preliminary) total $\Sigma^+ p$ cross sections from the recent KEK experiment E289 [24]. In Sec. VIII these are given together with the results. Next to these we added pseudodata for the Λp and $\Lambda\Lambda$ scattering lengths and effective ranges, in fm:

$$\begin{aligned} \hat{a}_{\Lambda p}({}^1S_0) &= -1.95 \pm 0.10, & \hat{r}_{\Lambda p}({}^1S_0) &= 2.90, \\ \hat{a}_{\Lambda p}({}^3S_1) &= -1.86 \pm 0.10, & \hat{r}_{\Lambda p}({}^3S_1) &= 2.70, \\ \hat{a}_{\Lambda\Lambda}({}^1S_0) &= -3.00 \pm 0.10, \end{aligned} \quad (31)$$

These Λp values are suggested by the experience in several hypernuclear applications of the NSC97 models. Also, during the fitting checks were done to prevent the occurrence of bound states. Parameters, typically strongly influenced by the YN data, are

- (i) $F/(F + D)$ parameters: $\alpha_{PV}, \alpha_V^m, \alpha_S,$
- (ii) SU(3) symmetry breaking: $\Delta_{\text{FSB}}.$

Notice that the strange octet mesons K , etc., were given the same form factors as their nonstrange companions. So, because of YN we have introduced four extra free parameters. We notice that the need to avoid bound states in the YN and YY systems has in particularly some influence on the trio $g_\epsilon, g_\omega,$ and g_P . Of particular importance of this was the introduction of the zero in the scalar-meson form factors, see part I for a detailed description. Like in part I, also here we used a fixed zero by taking $U = 750$ MeV.

VI. COUPLING CONSTANTS, $F/(F + D)$ RATIOS, AND MIXING ANGLES

Like in part I, we constrained the OBE couplings by the “naive” predictions of the QPC model [8]. We kept during the searches all OBE couplings in the neighborhood of these predictions, but a little less so than in part I. The same has been

TABLE III. Meson couplings and meson masses and cut-off parameters employed in the ESC04 potentials. Coupling constants are at $\mathbf{k}^2 = 0$. An asterisk denotes that the coupling constant is not searched, but constrained via SU(3) are simply put to some value used in previous work. The used widths of the ρ and ϵ are 146 and 640 MeV respectively.

Meson	Mass (MeV)	$g/\sqrt{4\pi}$	$f/\sqrt{4\pi}$	Λ (MeV)
π	138.04		0.2631	833.63
η	548.80		0.1933*	833.63
η	957.50		0.1191	900.00
ρ	770.00	0.7800	3.4711	839.53
ϕ	1019.50	-0.3788	-0.0494*	839.53
ω	783.90	3.0138	0.4467	869.84
a_1	1270.00	2.5426		945.66
f_1	1420.00	0.8896*		945.66
f'_1	1285.00	1.2544		945.66
a_0	962.00	0.9251		1159.88
f_0	993.00	-0.8162		1159.88
ϵ	760.00	3.4635		1101.61
a_2	309.10	0.0000		
f_2	309.10	0.0000		
f'_2	309.10	0.0000		
Pomeron	309.10	1.9651		

done for all $\alpha = F/(F + D)$ ratios, i.e., for BBM and the BB pair couplings. In fact, all $F/(F + D)$ ratios were fixed, except the ratio α_V^m for vector mesons and α_S for the scalar mesons.

The mixing for the pseudoscalar, vector, and scalar mesons, as well as the handling of the diffractive potentials, have been described elsewhere, see, e.g. [3,4]. The mixing, etc., of the axial-vector mesons is completely the same as for the vector, etc., mesons and therefore need not be discussed here.

In Table III we give the fitted ESC04 meson couplings and parameters.

In Table IV we compare the fitted meson coupling constants with the “naive” predictions of the QPC model. For the QPC predictions in Table IV; see part I. One sees that the fitted parameters are rather close to those of the QPC model and even more so than in paper part I. Notice that we omitted here the pion coupling, which requires a different γ_M factor in the QPC model; see remarks in part I. Also, we see that the deviation between the scalar and vector couplings from the QPC model relations, $g_\epsilon - g_\omega \approx 3(g_{a_0} - g_\rho)$, which seems a purely isospin factor.

In Table V the SU(3) singlet and octet couplings are listed, i.e., \hat{g} , etc., as well as $F/(F + D)$ ratios and mixing angles.

TABLE IV. $NN + YN$: ESC04 couplings and 3P_0 -model relations.

Meson	r_M [fm]	X_M	γ_M	3P_0	ESC04
$\rho(770)$	0.56	1/2	1.53	$g = 0.78$	$g = 0.78$
$\omega(783)$	0.56	3/2	1.53	$g = 2.40$	$g = 3.01$
$a_0(962)$	0.56	$\sqrt{3}/2$	1.53	$g = 0.79$	$g = 0.92$
$\epsilon(760)$	0.56	$3\sqrt{3}/2$	1.53	$g = 2.11$	$g = 3.46$
$a_1(1270)$	0.56	$3\sqrt{3}/2$	1.53	$g = 2.73$	$g = 2.54$

TABLE V. Coupling constants, $F/(F + D)$ ratios, mixing angles, etc. The values with a superscript a have been determined in the fit to the YN data. The other parameters are theoretical input or determined by the fitted parameters and the constraint from the NN analysis.

Mesons		{1}	{8}	$F/(F + D)$	Angles
ps-scalar	f	0.1852	0.2631	$\alpha_{PV} = 0.4668^a$	$\theta_P = -23.00^\circ$
Vector	g	2.6218	0.7800	$\alpha_V^c = 1.0$	$\theta_V = 37.50^\circ$
	f	0.3845	3.4711	$\alpha_V^m = 0.2760^a$	
Axial	g	1.5023	2.5426	$\alpha_A = 0.2340$	$\theta_A =$ -23.00^{oa}
Scalar	g	3.1688	0.9251	$\alpha_S = 0.8410$	$\theta_S = 40.32^{oa}$
Diffraction	g	1.9651	0.0000	$\alpha_D = 1.000$	$\psi_D = 0.0^{oa}$

In Tables VI and VII we list the couplings of the physical mesons to the nucleons ($Y = 1$), and the hyperons with $Y = 0$. These were computed using the FSB scheme, described above. We found (ESC04a) $\Delta_{\text{FSB}}(\text{PV}) = -0.258$ and $\Delta_{\text{FSB}}(V, S, A) = -0.267$.

In Table VIII we listed the fitted pair couplings for the MPE potentials. We recall that only one-pair graphs are included, to avoid double counting; see part I. The $F/(F + D)$ ratios are all fixed, assuming heavy-boson domination of the pair vertices. The ratios are taken from the QPC model for $Q\bar{Q}$ systems with the same quantum numbers as the dominating boson. The BB pair couplings are computed, assuming unbroken SU(3) symmetry, from the NN pair coupling and the $F/(F + D)$ ratio using SU(3).

Unlike in Ref. [17], we did not fix pair couplings using a theoretical model, based on heavy-meson saturation and chiral symmetry. So, in addition to the 14 parameters used in Ref. [17] we now have six pair-coupling fit parameters. In Table VIII the fitted pair couplings are given. Note that the $(\pi\pi)_0$ pair coupling gets contributions from the {1} and the {8_s} pairs as well, giving in total $g_{(\pi\pi)} = 0.10$, which has the same sign as

TABLE VI. Coupling constants for pseudoscalar and vector meson $Y = 0$ and $Y = \pm 1$ exchanges.

M		NNM	$\Lambda\Lambda M$	$\Lambda\Sigma M$	$\Sigma\Sigma M$	ΛNM	ΣNM
π	g	3.57602	CSB	2.47895	4.23203	—	—
	f	0.26306	CSB	0.16196	0.24559	—	—
η	f	0.19333	-0.02028	—	0.21534	—	—
	η'	f	0.11908	0.14213	—	0.11671	—
K	g	—	—	—	—	-3.22933	0.19837
	f	—	—	—	—	-0.21786	0.01296
ρ	g	0.78000	CSB	—	1.56000	—	—
	f	3.47113	CSB	2.90094	1.91768	—	—
ϕ	g	-0.37884	-0.94125	—	-0.94125	—	—
	f	-0.04944	-1.34461	—	1.07066	—	—
ω	g	3.01376	2.21121	—	2.21121	—	—
	f	0.44671	-1.40149	—	2.04507	—	—
K^*	g	—	—	—	—	-0.99079	-0.57203
	f	—	—	—	—	-2.28171	1.13927
a_1	g	2.54264	CSB	2.24770	1.19215	—	—
f_1	g	0.88961	-0.66726	—	2.57849	—	—
f_1'	g	1.25438	1.40489	—	1.09111	—	—
K_1	f	—	—	—	—	-1.58137	0.99042

TABLE VII. Coupling constants for scalar meson and “diffractive” $Y = 0$ and $Y = \pm 1$ exchanges. Nomenclature scalar mesons: $\delta = a_0(962)$, $\epsilon = f_0(760)$, $S^* = f_0(993)$, $\kappa = K_0^*(900)$.

M		NNM	$\Lambda\Lambda M$	$\Lambda\Sigma M$	$\Sigma\Sigma M$	ΛNM	ΣNM
δ	g	0.92511	CSB	0.16975	1.55621	—	—
S^*	g	-0.81620	-1.36993	—	-1.23870	—	—
ϵ	g	3.46354	2.58418	—	2.79258	—	—
κ	g	—	—	—	—	-1.05063	-0.46283
A_2	g	0.00000	CSB	0.00000	0.00000	—	—
P	g	1.96510	1.96510	—	1.96510	—	—
K_2^{**}	g	—	—	—	—	0.00000	0.00000

in Ref. [17]. The $f_{(\pi\pi)_1}$ pair coupling has opposite sign as compared to Ref. [17]. In a model with a more complex and realistic meson dynamics [25] this coupling is predicted as found in the present ESC fit. The $(\pi\rho)_1$ coupling agrees nicely with A_1 saturation; see Ref. [17]. We conclude that the pair couplings are in general not well understood and deserve more study.

In the ESC model described here, is fully consistent with SU(3) symmetry using a straightforward extension of the NN model to YN and YY . For example, $g_{(\pi\rho)_1} = g_{A_8 VP}$, and in addition to $(\pi\rho)$ pairs one sees also that $KK^*(I = 1)$ and $KK^*(I = 0)$ pairs contribute to the NN potentials. All $F/(F + D)$ ratios are taken fixed with heavy-meson saturation in mind. The approximation we have made in this article is to neglect the baryon mass differences, i.e., we put $m_\Lambda = m_\Sigma = m_N$. This because we have not yet worked out the formulas for the inclusion of these mass differences, which is straightforward in principle.

VII. ESC04 MODEL, NN RESULTS

A. Parameters and nucleon-nucleon fit

For a more detailed discussion on the NN fitting we refer to part I. Here, we fit only to the 1993 Nijmegen representation of the χ^2 hypersurface of the NN -scattering data below $T_{\text{lab}} = 350$ MeV [22,23]. This in contrast to part I where also low-energy parameters are fitted for $n\rho$ and nn . In this simultaneous fit of NN and YN , we obtained for the phase shifts a $\chi^2/N \text{ data} = 1.22$. In Table III the meson parameters are given for the ESC04a model. In Table IX the distribution of the χ^2 is shown for the 10 energy bins, which can be compared with a similar table in part I. Also, for a comparison with part I, and for use of this model for the description of NN , we give in

TABLE VIII. Pair-meson coupling constants employed in the ESC04 MPE potentials. Coupling constants are at $\mathbf{k}^2 = 0$.

J^{PC}	SU(3)-irrep	$(\alpha\beta)$	$g/4\pi$	$F/(F + D)$
0^{++}	{1}	$g_{(\pi\pi)_0}$	—	—
0^{++}	{1}	$g_{(\sigma\sigma)}$	—	—
0^{++}	{8 _s }	$g_{(\pi\eta)}$	-0.1860	1.000
1^{--}	{8 _a }	$g_{(\pi\pi)_1}$	-0.0024	1.000
		$f_{(\pi\pi)_1}$	0.1310	0.400
1^{++}	{8 _a }	$g_{(\pi\rho)_1}$	0.8864	0.643
1^{++}	{8 _a }	$g_{(\pi\sigma)}$	-0.0241	0.643
1^{++}	{8 _a }	$g_{(\pi P)}$	0.0	—
1^{+-}	{8 _s }	$g_{(\pi\omega)}$	-0.1722	0.467

TABLE IX. χ^2 and $\hat{\chi}^2$ per datum at the 10 energy bins for the Nijmegen93 partial-wave analysis. N_{data} lists the number of data within each energy bin. The bottom line gives the results for the total 0–350 MeV interval. The χ^2 access for the ESC04 model in the $NN + YN$ fit is denoted by $\Delta\chi^2$ and $\Delta\hat{\chi}^2$, respectively.

T_{lab}	# data	χ_0^2	$\Delta\chi^2$	$\hat{\chi}_0^2$	$\Delta\hat{\chi}^2$
0.383	144	137.5549	22.9	0.960	0.159
1	68	38.0187	53.2	0.560	0.783
5	103	82.2257	7.1	0.800	0.068
10	209	257.9946	53.1	1.234	0.183
25	352	272.1971	62.5	0.773	0.177
50	572	547.6727	240.3	0.957	0.420
100	399	382.4493	73.6	0.959	0.184
150	676	673.0548	104.4	0.996	0.154
215	756	754.5248	214.4	0.998	0.284
320	954	945.3772	333.1	0.991	0.349
Total	4233	4091.122	1164.6	0.948	0.268

Tables X and XI the nuclear-bar phases for pp in case $I = 1$ and for np in case $I = 0$. The deuteron was not fitted, and we have for the binding energy $E_B = 2.224797$ MeV, which is very close to the $E_B(\text{experiment}) = 2.224644$.

VIII. ESC04 MODEL, YN RESULTS

In combined NN and YN fit, the used YN -scattering data from Refs. [26–31], are shown in Table XII. Because we know from the experience with the NSC97 models rather well the favored s -wave scattering lengths for ΛN , we added values for these as pseudodata, see Sec. V B. The NN interaction puts very strong constraints on most of the parameters, and so we are left with only a limited set of parameters which have some freedom to steer the YN channels. Like in the NSC97 models

TABLE X. ESC04 pp and np nuclear-bar phase shifts in degrees.

T_{lab}	0.38	1	5	10	25
# data	144	68	103	290	352
$\Delta\chi^2$	24	53	7	53	62
1S_0	14.62	32.62	54.71	55.07	48.39
3S_1	159.39	147.77	118.23	102.70	80.78
ϵ_1	0.03	0.11	0.66	1.13	1.71
3P_0	0.02	0.13	1.56	3.69	8.58
3P_1	-0.01	-0.08	-0.87	-2.01	-4.85
1P_1	-0.05	-0.19	-1.52	-3.12	-6.46
3P_2	0.00	0.01	0.21	0.64	2.44
ϵ_2	-0.00	-0.00	-0.05	-0.19	-0.79
3D_1	0.00	-0.01	-0.19	-0.69	-2.85
3D_2	0.00	0.01	0.22	0.85	3.72
1D_2	0.00	0.00	0.04	0.16	0.67
3D_3	0.00	0.00	0.00	0.00	0.01
ϵ_3	0.00	0.00	0.01	0.08	0.56
3F_2	0.00	0.00	0.00	0.01	0.10
3F_3	0.00	0.00	-0.00	-0.03	-0.22
1F_3	0.00	0.00	-0.01	-0.07	-0.42
3F_4	0.00	0.00	0.00	0.00	0.02
ϵ_4	0.00	0.00	0.00	-0.00	-0.05

TABLE XI. ESC04 pp and np nuclear-bar phase shifts in degrees.

T_{lab}	50	100	150	215	320
# data	572	399	676	756	954
$\Delta\chi^2$	240	74	104	214	333
1S_0	38.40	24.05	13.51	2.79	-10.60
3S_1	63.01	43.67	31.44	19.93	6.42
ϵ_1	1.94	2.18	2.56	3.22	4.57
3P_0	11.65	9.84	5.19	-1.31	-10.86
3P_1	-8.23	-13.19	-17.25	-21.85	-28.09
1P_1	-9.75	-14.12	-17.78	-22.09	-28.12
3P_2	5.75	11.02	14.21	16.29	16.96
ϵ_2	-1.68	-2.68	-2.97	-2.83	-2.17
3D_1	-6.58	-12.61	-17.06	-21.36	-26.14
3D_2	8.92	17.08	21.90	24.70	24.83
1D_2	1.66	3.80	5.88	8.09	10.16
3D_3	0.18	1.05	2.15	3.42	4.60
ϵ_3	1.62	3.52	4.88	6.02	6.97
3F_2	0.32	0.74	0.98	0.97	0.13
3F_3	-0.66	-1.46	-2.09	-2.74	-3.73
1F_3	-1.13	-2.20	-2.90	-3.58	-4.65
3F_4	0.10	0.42	0.88	1.57	2.71
ϵ_4	-0.19	-0.52	-0.81	-1.12	-1.46
3G_3	-0.27	-0.99	-1.89	-3.10	-4.88
3G_4	0.72	2.13	3.54	5.16	7.23
1G_4	0.15	0.40	0.65	1.00	1.60
3G_5	-0.06	-0.21	-0.36	-0.49	-0.58
ϵ_5	0.21	0.72	1.26	1.91	2.75

we exploit here (i) the magnetic vector-meson $F/(F + D)$ ratio α_V^m , (ii) the scalarmeson $F/(F + D)$ ratio α_S , and the flavor-symmetry-breaking parameter Δ_{FSB} . We did not break $SU(3)$ by introducing independent cutoff parameters for the strange mesons K, K^* , etc., but $\Lambda_K = \Lambda_\pi$ and similar for the other meson nonets. The fitted parameters are given in Tables III and VIII.

The aim of the present study was to construct a realistic potential model for baryon-baryon with parameters that are optimal theoretically, but at the sametime describes the baryon-baryon scattering data very satisfactory.

This model can then be used with a great deal of confidence in calculations of hypernuclei and in their predictions for the $S = -2, -3$, and -4 sectors. Especially for the latter application, these models will be the first models for the $S < -1$ sector to have their theoretical foundation in the NN and YN sectors.

The χ^2 on the 38 YN -scattering data for the ESC04 model is given in Table XII. The capture ratio at rest, given in the last column of the table, for its definition see, e.g., Ref. [4]. This capture ratio turns out to be rather constant in the momentum range from 100 to 170 MeV/c. Obviously, for very low momenta the cross sections are almost completely dominated by S waves. For a discussion of the capture ratio at rest r_R ; see Ref. [32–34]. We obtained $r_R = 0.473$, which is close to the experimental value $r_R^{\text{exp}} = 0.468 \pm 0.010$.

The $\Sigma^+ p$ nuclear-bar phase shifts as a function of energy are given in Table XIII. Notice that the 3S_1 phase shows repulsion, except for very low energies. This means that the the potential has a weak long range attractive tail.

TABLE XII. Comparison of the calculated and experimental values for the 38 YN data that were included in the fit. The superscripts RH and M denote, respectively, the Rehovoth-Heidelberg Ref. [26] and Maryland data Ref. [27]. Also included are 3 Σ^+p cross sections at $p_{\text{lab}} = 400, 500,$ and 650 MeV from Ref. [23]. The laboratory momenta are in MeV/nucleon, and the total cross sections in mb.

$\Lambda p \rightarrow \Lambda p$			$\Lambda p \rightarrow \Lambda p$		
p_{Λ}	$\sigma_{\text{exp}}^{\text{RH}}$	σ_{th}	p_{Λ}	σ_{exp}^M	σ_{th}
145	180±22	182.1	135	209.0±58	195.6
185	130±17	135.7	165	177.0±38	157.4
210	118±16	112.6	195	153.0±27	125.9
230	101±12	97.1	225	111.0±18	100.8
250	83±9	84.4	255	87.0±13	81.0
290	57±9	63.2	300	46.0±11	59.0
$\chi^2 = 0.8$			$\chi^2 = 3.3$		
$\Sigma^+p \rightarrow \Sigma^+p$			$\Sigma^-p \rightarrow \Sigma^-p$		
p_{Σ^+}	σ_{exp}	σ_{th}	p_{Σ^-}	σ_{exp}	σ_{th}
145	123±62	104.3	142.5	152±38	133.7
155	104±30	94.3	147.5	146±30	128.9
165	92±18	85.4	152.5	142±25	124.4
175	81±12	77.4	157.5	164±32	120.0
400	75±25	26.6	162.5	138±19	115.9
500	26±20	24.9	167.5	113±16	111.9
650	52±40	21.9			
$\chi^2 = 4.7$			$\chi^2 = 4.3$		
$\Sigma^-p \rightarrow \Sigma^0n$			$\Sigma^-p \rightarrow \Lambda n$		
p_{Σ^+}	σ_{exp}	σ_{th}	p_{Σ^-}	σ_{exp}	σ_{th}
110	396±91	183.2	110	174±47	219.9
120	159±43	160.0	120	178±39	188.7
130	157±34	141.1	130	140±28	163.6
140	125±25	125.5	140	164±25	143.0
150	111±19	112.3	150	147±19	126.0
160	115±16	101.1	160	124±14	111.7
$r_R^{\text{exp}} = 0.468 \pm 0.010$			$r_R^{\text{th}} = 0.473$		
			$\chi^2 = 0.2$		

The ΛN nuclear-bar phase shifts as a function of energy are given in Table XIV. The 3S_1 phase shows that there is a resonance below the ΣN threshold, the so-called analog of the

 TABLE XIV. ESC04 nuclear-bar Λp phases in degrees.

p_{Λ}	100	200	300	400	500	600	633.4
T_{lab}	4.5	17.8	39.6	69.5	106.9	151.1	167.3
1S_0	22.30	29.20	27.49	22.59	16.68	10.62	8.65
3S_1	17.72	26.17	28.37	28.95	32.25	55.52	102.55
ϵ_1	0.07	0.30	0.48	0.25	-1.18	-8.43	17.32
3P_0	0.03	0.15	0.06	-0.79	-2.74	-5.66	-6.76
1P_1	-0.02	-0.12	-0.52	-1.45	-3.01	-5.09	-5.86
3P_1	0.03	0.13	0.14	-0.17	-0.90	-1.93	-2.23
3P_2	0.13	0.89	2.41	4.32	6.10	7.47	7.84
ϵ_2	0.00	0.00	-0.04	-0.14	-0.30	-0.52	-0.64
3D_1	0.00	0.02	0.12	0.40	1.04	3.11	2.19
1D_2	0.00	0.07	0.24	0.74	1.54	2.51	2.84
3D_2	0.00	0.06	0.30	0.82	1.62	2.53	2.82

deuteron. This signals the fact that in the $\Sigma N({}^3S_1, I = 1/2)$ state there is a strong attraction.

In Fig. 6 we plot the total potentials for the S -wave channels $\Lambda N \rightarrow \Lambda N$, $\Lambda N \rightarrow \Sigma N$, and $\Sigma N \rightarrow \Sigma N$. The same is done in Figs. 7, 8, and 9 for respectively the OBE, TME, and MPE contributions. In Figs. 10 and 11 we show for the same

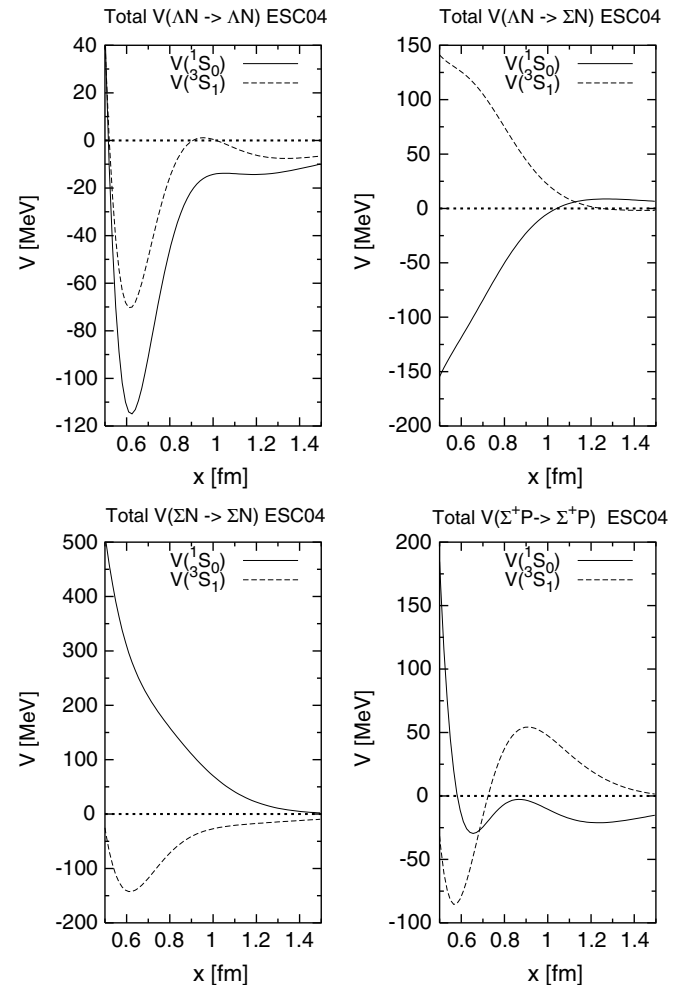

 FIG. 6. Total potentials in the partial waves 1S_0 and 3S_1 , for the $I = 1/2$ and $I = 3/2$ states.

 TABLE XIII. ESC04 nuclear-bar Σ^+p phases in degrees.

p_{Σ^+}	200	400	600	800	1000
T_{lab}	16.7	65.5	142.8	244.0	364.5
1S_0	39.05	26.07	10.11	-4.50	-17.46
3S_1	1.26	-0.21	-3.75	-6.80	-10.11
ϵ_1	-3.38	-4.54	-2.89	0.57	3.82
3P_0	5.91	10.76	3.87	-7.62	-19.84
1P_1	4.62	21.50	35.55	38.36	35.06
3P_1	-3.28	-9.20	-13.96	-17.52	-19.59
3P_2	1.29	7.61	14.89	19.30	20.58
ϵ_2	-0.44	-1.26	-2.72	-2.61	-0.20
3D_1	0.34	1.54	1.73	-0.63	-5.70
1D_2	0.36	2.22	5.276	8.20	9.51
3D_2	-0.53	-2.81	-5.48	-8.49	-11.95
3D_3	0.06	0.97	3.18	5.91	8.40

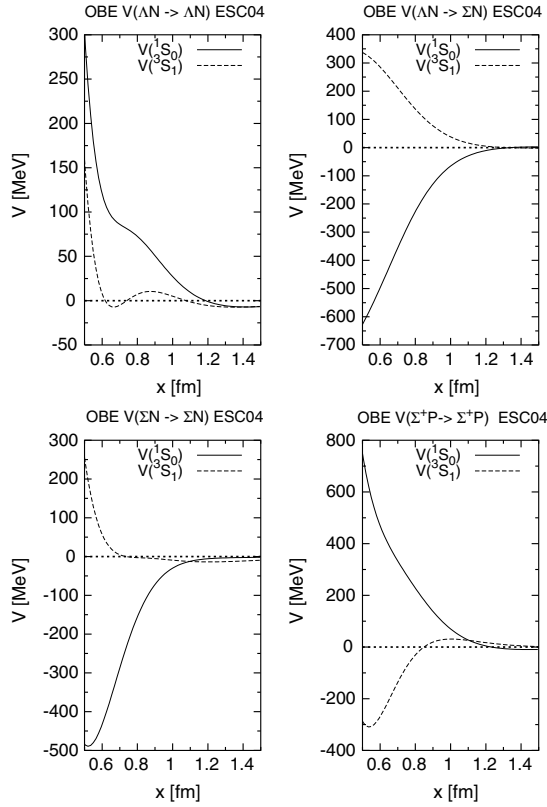


FIG. 7. OBE potentials in the partial waves 1S_0 and 3S_1 , for the $I = 1/2$ and $I = 3/2$ states.

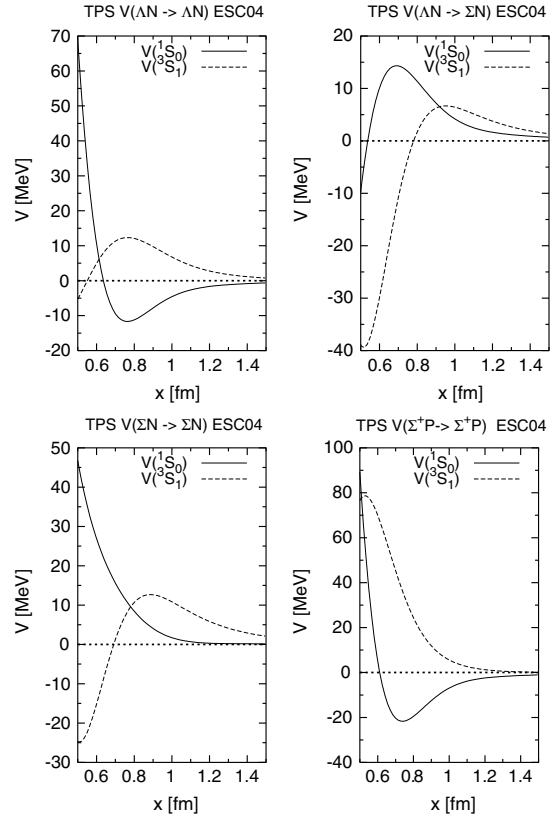


FIG. 8. TPS potentials in the partial waves 1S_0 and 3S_1 , for the $I = 1/2$ and $I = 3/2$ states.

channels the OBE contributions from the different types of mesons: The pseudoscalar, the vector, the scalar, and the axial-vector mesons. From these figures one can notice e.g. (i) the total potentials are dominated by the OBE and MPE contributions and (ii) the OBE and MPE potentials are often opposite to each other. For example, the ΔN elastic potentials are attractive because of the sizable attractive contributions from the MPE potentials overcoming the OBE ones.

Finally, all ESC potentials described in this article are available on the Internet [35].

IX. BRIEF COMPARISON ESC04 MODELS

In this section we display some global comparison between the different ESC04a–d models emerging from the different options, mentioned above.

In Table XV we give the FSB and a_{PV} parameters and the χ^2 obtained in the simultaneous $NN \oplus YN$ fitting.

TABLE XV. Δ_{FSB^-} , a_{PV} parameters, and the χ^2 s for NN and YN .

	a_{PV}	$\Delta_{FSB}(PV)$	$\Delta_{FSB}(V)$	$\chi^2_{p.d.p.}(NN)$	$\chi^2(YN)$
ESC04a	0.5	-0.258	-0.267	1.22	24.2
ESC04b	1.0	-0.214	-0.280	1.20	49.5
ESC04c	0.5	0.000	0.000	1.28	23.0
ESC04d	1.0	0.000	0.000	1.33	26.0

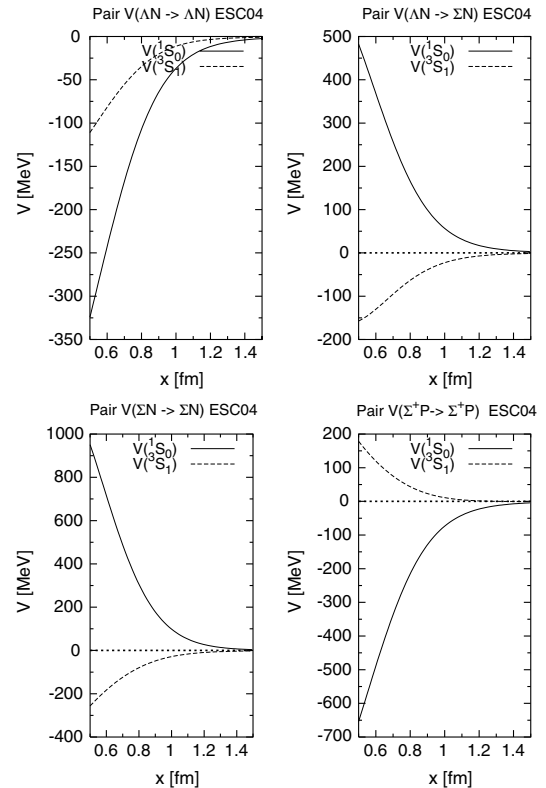


FIG. 9. Pair potentials in the partial waves 1S_0 and 3S_1 , for the $I = 1/2$ and $I = 3/2$ states.

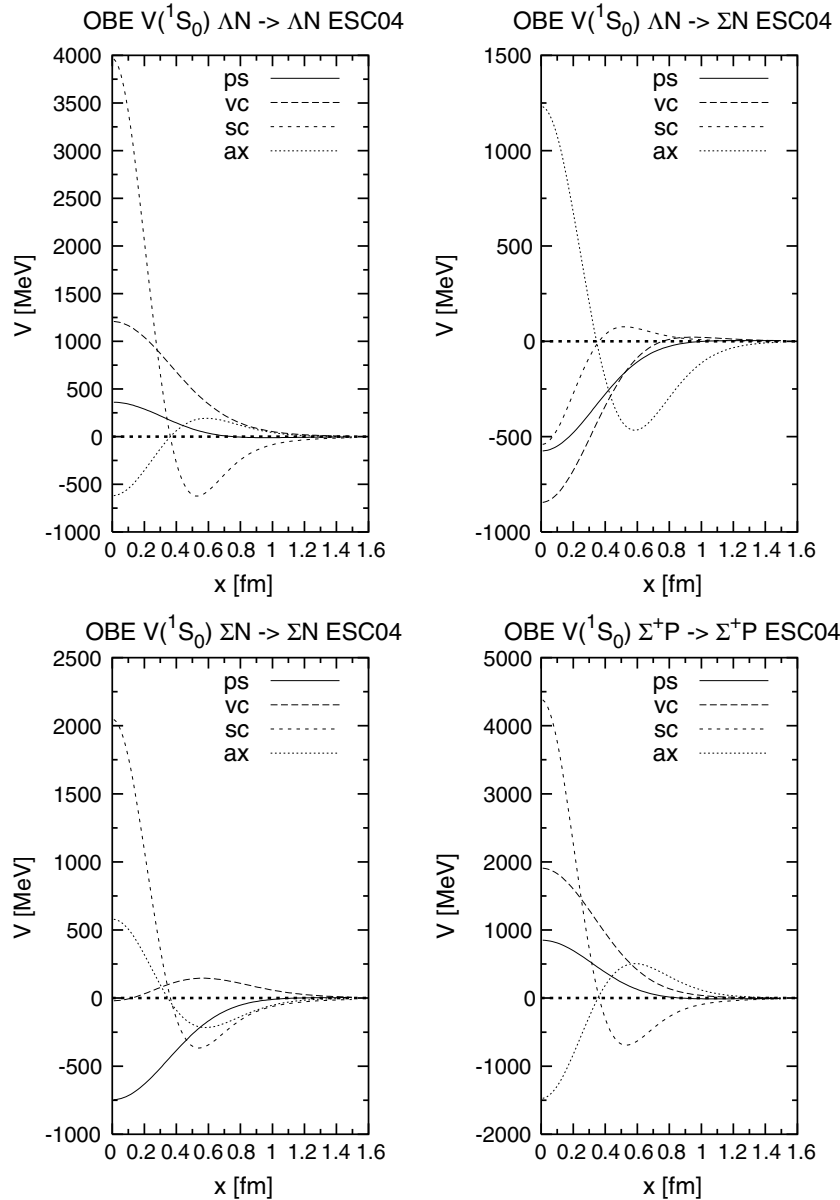


FIG. 10. OBE potentials in the 1S_0 partial waves, for pseudoscalar (PS), vector (VC), scalar (SC), and axial-vector (AX) exchange, in the $I = 1/2$ and $I = 3/2$ states.

In Table XVI we give the $F/(F + D)$ ratios and θ_S . The latter because in these models there is no imposed constraint on the parameters (α_S, θ_S) . The vector mixing angle θ_V is for all models the same. This is also the case for the axial mixing angle where we fixed $\theta_A = \theta_{PS} = -23.0^\circ$. In this table it is remarkable that, whereas α_S is constant, there is a big difference with respect to θ_S . Furthermore, one notices that

TABLE XVI. $F/(F + D)$ ratios for OBE couplings, and the scalar-meson mixing angle θ_S in degrees.

	α_{PV}	α_V^e	α_V^m	α_A	α_S	θ_S
ESC04a	0.467	1.0	0.276	0.234	0.841	40.32
ESC04b	0.403	1.0	0.316	0.246	0.841	40.31
ESC04c	0.510	1.0	0.306	0.234	0.841	22.09
ESC04d	0.499	1.0	0.430	0.234	0.841	11.45

for most models α_V^m is close to the estimates from static and nonstatic SU(6) [36]. As a final point we mention that the $F/(F + D)$ ratios for the pair couplings are very similar to the values of ESC04b, given above.

In Table XVII we list the ΛN -scattering lengths and effective ranges. Here, (a_s, r_s) are these quantities for $\Lambda N(^1S_0)$ and (a_t, r_t) for $\Lambda N(^3S_1)$. Here we repeat the different options used to distinguish the different models.

TABLE XVII. ΛN scattering lengths and effective ranges in fm.

	SFB	a_{PV}	a_s	a_t	r_s	r_t
ESC04a	yes	0.5	-2.073	-1.537	2.998	2.773
ESC04b	yes	1.0	-1.957	-1.689	3.156	2.823
ESC04c	no	0.5	-1.946	-1.850	3.473	2.900
ESC04d	no	1.0	-1.941	-1.858	3.570	3.133

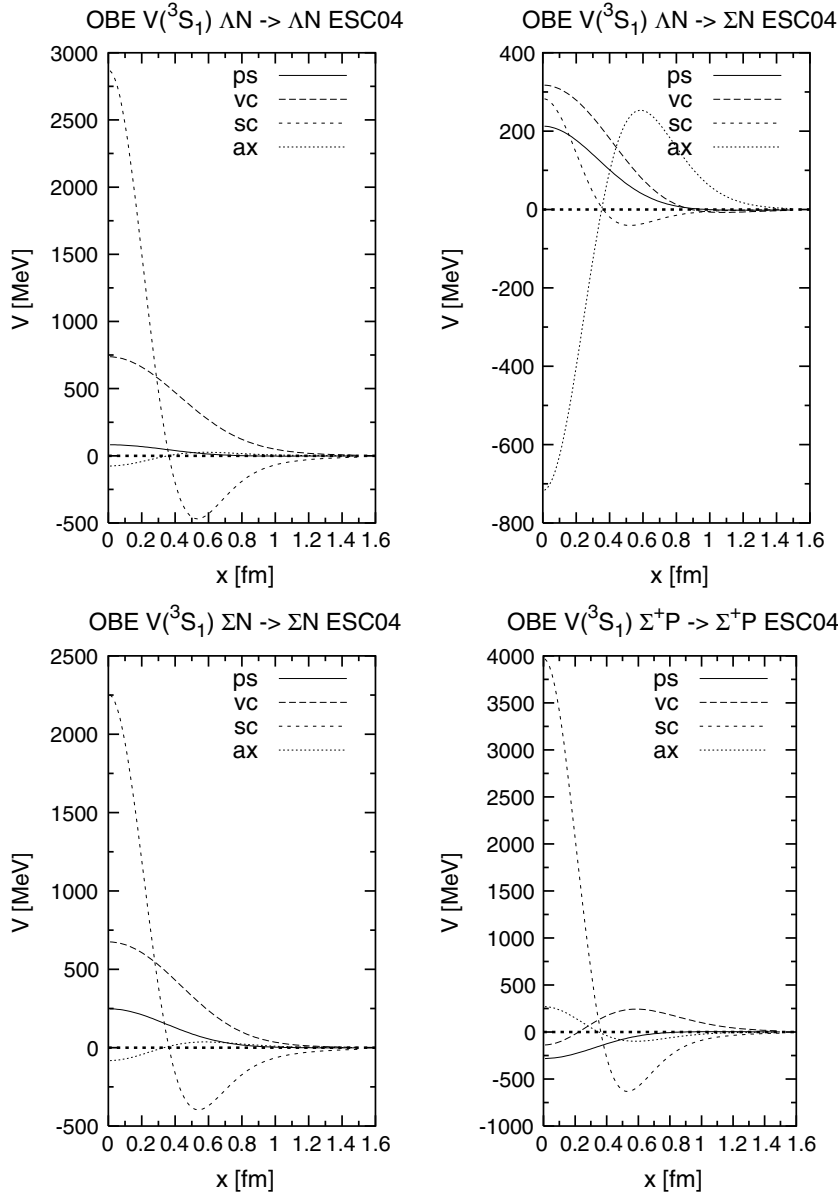


FIG. 11. OBE potentials in the 3S_1 partial waves, for pseudoscalar (PS), vector (VC), scalar (SC), and axial-vector (AX) exchange, in the $I = 1/2$ and $I = 3/2$ states.

In Table XVIII we list the scattering lengths and effective ranges for Σ^+p and $\Lambda\Lambda$.

X. G-MATRIX INTERACTIONS AND HYPERNUCLEI

A. Properties of ΛN and ΣN G matrices

The free-space YN -scattering data are too sparse to discriminate clearly the YN interaction models. Then, it is very

TABLE XVIII. Σ^+p and $\Lambda\Lambda$ scattering lengths and effective ranges in fm.

	a_s	a_t	r_s	r_t	$a_s(\Lambda\Lambda)$	$r_s(\Lambda\Lambda)$
ESC04a	-4.09	-0.020	3.49	-3356	-1.149	4.482
ESC04b	-2.87	+0.179	4.10	-34.20	-1.245	4.453
ESC04c	-3.87	+0.077	3.72	-253.5	-1.081	4.463
ESC04d	-3.43	+0.217	3.98	-28.94	-1.323	4.401

helpful to test the interaction models in analyses of various hypernuclear phenomena. Effective YN interactions used in models of hypernuclei can be derived from the free-space YN interactions most conveniently using the G -matrix theory. In the previous work [4], the G -matrix results were used as an important guidance to discriminate especially the spin-dependent parts in the interaction models. Here, the versions $a \sim f$ of the NSC97 model were designed so as to specify their different strengths of ΛN spin-spin interactions, and among them those of NSC97e and NSC97f were demonstrated to be consistent with the hypernuclear data. Afterwards, the plausibility of our approach has been confirmed by successful calculations for s -shell hypernuclei [37–39] using NSC97e/f or their simulated versions.

Let us perform the G -matrix analyses for ESC04a–d in the same way. The G -matrix equations for YN pairs in nuclear matter are solved with the simple QTQ prescription (the gap choice) for the intermediate-state spectra, which means that no

TABLE XIX. Values of U_Λ at normal density and partial wave contributions for ESC04a–d and NSC97e/f obtained from the G -matrix calculations with the QTQ intermediate spectra. All entries are in MeV.

	1S_0	3S_1	1P_1	3P_0	3P_1	3P_2	D	U_Λ
ESC04a	-13.7	-20.5	0.6	0.2	0.5	-4.5	-1.0	-38.5
ESC04b	-13.3	-22.6	0.5	-0.0	0.6	-4.3	-1.1	-40.2
ESC04c	-13.9	-28.5	2.9	0.0	1.3	-6.5	-1.3	-46.0
ESC04d	-13.6	-26.6	3.2	-0.2	0.9	-6.4	-1.4	-44.1
NSC97e	-12.7	-25.5	2.1	0.5	3.2	-1.3	-1.2	-34.8
NSC97f	-14.3	-22.4	2.4	0.5	4.0	-0.7	-1.2	-31.8

potential term is taken into account in the off-shell propagation. As discussed for NSC97 [4], the QTQ prescription is accurate enough to investigate properties of YN G -matrix interactions. The nucleon energy spectra in the YN G -matrix equation are obtained from the NN G matrices for ESC04(NN), where the phenomenological three-nucleon interaction (TNI) is taken into account so as to assure nuclear saturation. The details for TNI are explained in the next subsection.

In this work, the properties of the G -matrix interactions derived from ESC04a–d models are compared often with those of NSC97e/f. The calculated values for NSC97e/f in this work are slightly different from those in Ref. [4] because of different choice of the nucleon spectra. Hereafter, a two-particle state with isospin (T), spin (S), orbital and total angular momenta (L and J) is represented as $^{2T+1,2S+1}L_J$. An isospin quantum number is often omitted, when it is evident.

In Table XIX we show the potential energies U_Λ for a zero-momentum Λ and their partial-wave contributions $U_\Lambda(^{2S+1}L_J)$ at normal density ρ_0 ($k_F = 1.35 \text{ fm}^{-1}$). A statistical factor $(2J+1)$ is included in $U_\Lambda(^{2S+1}L_J)$. The total contributions U_Λ should be compared to the experimental value of about -30 MeV. In an appearance, the values for ESC04a–d seem to be rather worse than those for NSC97e/f. It should be noted, however, that the shallower values of U_Λ for NSC97e/f are owing to the strongly repulsive contributions of their P -state interactions. The sums of even-state contributions for ESC04a/b (ESC04c/d) are similar to (slightly larger than) those for NSC97e/f. One should notice here that the even-state strengths of NSC97e/f are proved to be attractive enough to reproduce appropriately Λ binding energies in s -shell hypernuclei [37–39]. Thus, we can say that the remarkable difference between ESC04a–d and NSC97e/f appears in the P -state interactions: Those of ESC04a–d and NSC97e/f are attractive and repulsive, respectively. If the attractive P -state interactions of ESC04a–d are considered to be reasonable, one should take into account another repulsive contribution to reproduce the value of $U_\Lambda \sim -30$ MeV, as discussed later. Though there are no clear-cut data for ΛN P -state interactions, an important consideration was given by Millener, supporting attractive P -state interactions [40]. He claims that the attractive P -state interaction is consistent with the 6.0 MeV separation observed in the (K^-, π^-) reaction for the two $(1/2^-)$ states of ^{13}C composed of the $^{12}\text{C}(0^+, 2^+) \otimes p_\Lambda$ configurations.

TABLE XX. Contributions to U_Λ at normal density from spin-independent, spin-spin, LS, and tensor parts of the G -matrix interactions derived from ESC04a–d and NSC97e/f. All entries are in MeV.

	$U_0(S)$	$U_{\sigma\sigma}(S)$	$U_0(P)$	$U_{\sigma\sigma}(P)$	$U_{LS}(P)$	$U_T(P)$
ESC04a	-8.55	1.73	-0.27	-0.25	-0.45	0.08
ESC04b	-8.96	1.44	-0.27	-0.22	-0.41	0.10
ESC04c	-10.6	1.09	-0.19	-0.86	-0.65	0.18
ESC04d	-10.1	1.19	-0.20	-0.96	-0.58	0.17
NSC97e	-9.55	1.06	0.38	-0.44	-0.46	0.17
NSC97f	-9.18	1.71	0.52	-0.50	-0.48	0.23

To see the spin-dependent features of the ΛN G -matrix interactions more clearly, it is convenient to derive contributions to U_Λ from the spin-independent, spin-spin, LS, and tensor components of the G matrices, which are denoted as $U_0, U_{\sigma\sigma}, U_{LS}, U_T$, respectively. These quantities in S and P states can be transformed from values of $U_\Lambda(^{2S+1}L_J)$ using Eq. (7.1) in Ref. [4]. The obtained values are shown in Table XX. The S -state contributions $U_0(S)$ for ESC04a–d are found to be not remarkably different from those for NSC97e/f. The relative ratio of $U_\Lambda(^1S_0)$ and $U_\Lambda(^3S_1)$ is related to the contribution $U_{\sigma\sigma}(S)$ from the spin-spin interaction. Various analyses suggest that the reasonable strength of the S -state spin-spin interaction is between those of NSC97e/f. Then, the spin-spin parts of ESC04a–d are found to be in this region, though they are slightly different from each other.

The features of the P -state interactions are indicated by the values of $U_0(P), U_{\sigma\sigma}(P), U_{LS}(P)$, and $U_T(P)$ in Table XX. The negative (positive) values of $U_0(P)$ for ESC04a–d (NSC97e/f) are because of the attractive (repulsive) interactions. The spin-spin, LS, and tensor strengths of ESC04a/b are slightly weaker than those of NSC97e/f. However, the spin-spin and LS strengths of ESC04c/d are rather stronger than the others. Let us discuss here the LS parts more in detail, because the clear data of the spin-orbit splittings have been obtained in the γ -ray experiments. The values of $U_{LS}(P)$ are composed of the contributions of two-body SLS interaction (attractive) and ALS interaction (repulsive). To compare clearly the SLS and ALS components, it is convenient to derive the strengths of the Λ l - s potentials in hypernuclei. In the same way as in Ref. [4], we use the following expression derived with the Scheerbaum approximation [41],

$$\begin{aligned}
 U_\Lambda^{ls}(r) &= K_\Lambda \frac{1}{r} \frac{d\rho}{dr} \mathbf{l} \cdot \mathbf{s}, \\
 K_\Lambda &= -\frac{\pi}{3} (S_{\text{SLS}} + S_{\text{ALS}}), \\
 S_{\text{SLS,ALS}} &= \frac{3}{\bar{q}} \int_0^\infty r^3 j_1(\bar{q}r) G_{\text{SLS,ALS}}(r) dr,
 \end{aligned} \tag{32}$$

where $G_{\text{SLS}}(r)$ and $G_{\text{ALS}}(r)$ are SLS and ALS parts of G -matrix interactions in configuration space, respectively, and $\rho(r)$ is a nuclear density distribution. We take here $\bar{q} = 0.7 \text{ fm}^{-1}$. Table XXI shows the values of K_Λ and $S_{\text{SLS,ALS}}$ obtained from the SLS and ALS parts of the ΛN G -matrix interactions calculated at $k_F = 1.0 \text{ fm}^{-1}$ in the cases of ESC04a–d and NSC97e/f. It is found here that the obtained

TABLE XXI. Strengths of Λ spin-orbit splittings for ESC04a–d and NSC97e/f. See the text for the definitions of K_Λ and $S_{\text{SLS,ALS}}$.

	S_{SLS}	S_{ALS}	K_Λ
ESC04a	−24.9	12.1	13.4
ESC04b	−22.3	13.2	9.5
ESC04c	−36.6	10.2	27.6
ESC04d	−32.7	10.1	23.6
NSC97e	−26.0	9.8	16.9
NSC97f	−26.9	9.5	18.1

values for ESC04a/b are smaller than those for NSC97e/f, because the SLS (ALS) parts of the former are less attractive (more repulsive) than those of the latter. However, the spin-orbit strengths of ESC04c/d are rather stronger than the others. In comparison of the experimental data, even the smallest K_Λ value in the case of ESC04b is too large [42,43].

In Fig. 12, the calculated values of U_Λ are drawn as a function of ρ/ρ_0 up to the high-density region. Their S and P contributions are shown in the left and right sides of Fig. 13, respectively. In these figures, solid, dashed, dotted, and dot-dashed curves are for ESC04a–d, respectively. For comparison, the result for NSC97f is drawn by the thin dashed curve. The U_Λ values for ESC04a–d are found to become far more attractive with increase of density than those of NSC97f. Comparing the partial-wave contributions for ESC04a–d with those for NSC97f, we find that the S -state contributions are more or less similar to each other and the distinct difference comes from the P -state contributions. The difference between the P -state interactions in ESC04 and NSC97 models turn out to be magnified dramatically in the high-density region.

The Λ effective mass M_Λ^* in nuclear matter is an important quantity that is related to the property of the underlying ΛN interaction. Here, we calculate a global effective mass defined

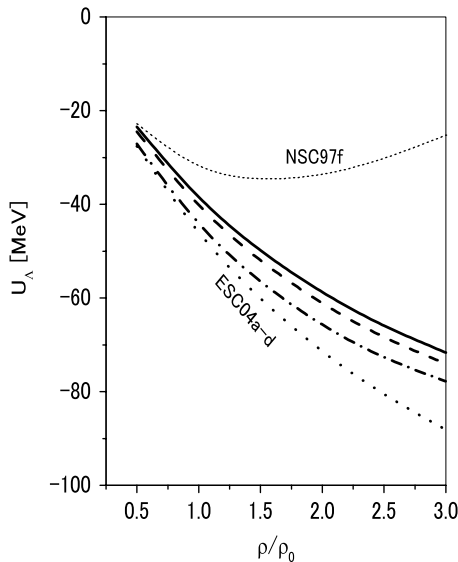


FIG. 12. Calculated values of U_Λ as a function of ρ/ρ_0 for ESC04a (solid curve), ESC04b (dashed curve), ESC04c (dotted curve), and ESC04d (dot-dashed curve). The thin dashed curve is for NSC97f.

by

$$\frac{M_\Lambda^*}{M_\Lambda} = \left(1 + \frac{dU_\Lambda}{dT_\Lambda}\right)^{-1}, \quad (33)$$

where T_Λ denotes Λ kinetic energy. The calculated values of $m_\Lambda^* = M_\Lambda^*/M_\Lambda$ at normal density are 0.81 (ESC04a), 0.79 (ESC04b), 0.77 (ESC04c), 0.74 (ESC04d), 0.67 (NSC97e), and 0.66 (NSC97f). In Fig. 14 the calculated values of m_Λ^* are drawn as a function of ρ/ρ_0 by solid (ESC04a), dashed (ESC04b), dotted (ESC04c), and dot-dashed (ESC04d) curves. The thin dashed curve is for NSC97f. We find here that the calculated values for NSC97f are distinctively smaller than the values for ESC04a–d. The reason why the m_Λ^* values for NSC97e/f are small is because their repulsive P -state interactions contribute to the derivatives dU_Λ/dT_Λ as large positive quantities. In Ref. [44], one of authors (Y.Y.) and collaborators analyzed the measured Λ -energy spectra in heavy hypernuclei with special attention to Λ effective masses. They concluded that the small value of m_Λ^* obtained from NSC97f leads to too broad level distances, and the adequate value of m_Λ^* is around 0.8 at normal density. Thus, the m_Λ^* values for ESC04a–d turn out to be more reasonable than those for NSC97 models.

Next, let us show the properties of ΣN G -matrix interactions. We solve here the ΣN starting channel G -matrix equation in the QTQ prescription. In this treatment, there appears no imaginary part, because of an energy-conserving $\Sigma N - \Lambda N$ transition. Although it is possible to derive the Σ conversion width Γ_Σ by taking into account the Λ and N potentials in the intermediate states, we choose not to discuss this rather complex issue in this article. In Table XXII we show the calculated values of U_Σ at normal density for ESC04a–d and NSC97f. Here, the U_Σ values for ESC04a–d are found to be far more attractive than that for NSC97f, because the $^3S_1(\Sigma N, I = 1/2)$ [$^1S_0(\Sigma N, I = 1/2)$] contributions for the former are remarkably more attractive (less repulsive) than that for the latter.

It has been pointed out that the Σ wells in nuclei might actually be repulsive, based on the Σ -atomic data [45] and the quasifree spectrum of the (K^-, π) reaction [46]. Recently, the (π^-, K^-) experiment has been performed to study the Σ -nucleus potentials [47]. They demonstrated that the observed spectrum can be reproduced with a strongly repulsive potential. The theoretical analyses for this data also indicate that the Σ -nucleus potential most likely is repulsive [48]. If we consider these analyses seriously, it is rather problematic how to understand repulsive Σ -nucleus potentials on the basis of the ESC model. It should be noted, however, that there is no decisive evidence for the repulsive Σ -nucleus potential experimentally in the present.

B. Three-body and nuclear medium effects

A natural possibility is the presence of three-body forces (3BF) in hypernuclei generating effective two-body forces, which could (partially) solve this well-depth issue. Because a thorough investigation is outside the scope of this article, we discuss three-body and nuclear medium effects here in a simple phenomenological way. As discussed in, for example,

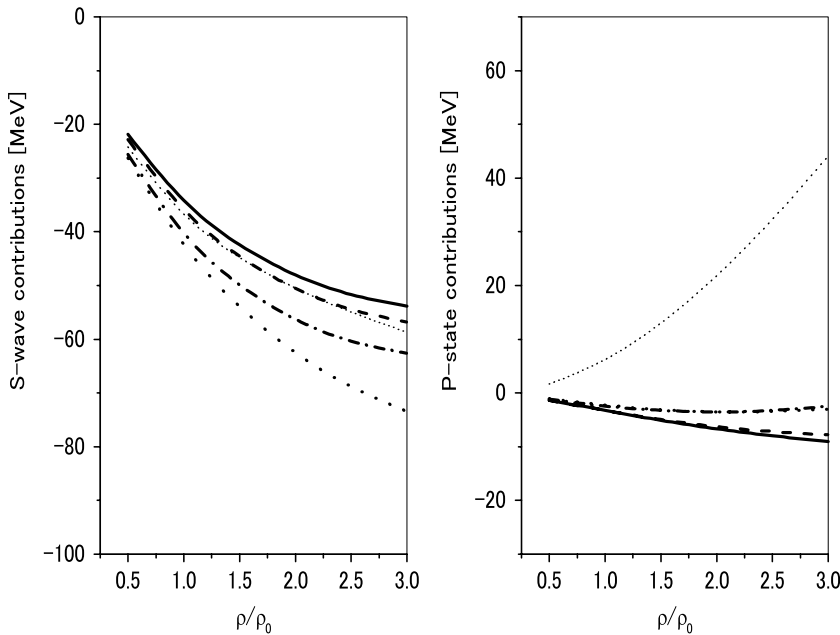


FIG. 13. S - and P -state contributions to U_Λ are shown in the left and right panels, respectively, as a function of ρ/ρ_0 . The solid, dashed, dotted, and dot-dashed curves are for ESC04a–d, respectively. The thin dashed curve is for NSC97f.

Ref. [49], three-body effects in a nuclear medium could be described roughly by using effective triple-meson vertices, like in Fig. 15. Here, the meson lines could be, e.g., scalar, vector, pomeron exchanges, etc. In view of the big cancellations in the two-body case for $\omega + P + \epsilon$ potentials, one expects also similar cancellations to take place in Fig. 15. One also expects that the density-dependent corrections in the nuclear medium give intermediate range (weak) attraction and short-range repulsion. In this short and simple discussion of the possible implications, we only consider the repulsive component. Figure 15 could be viewed on as the exchange of a meson between two-nucleons, whereas it is scattered intermediately by a third one. Then, it is natural to describe such an effect by a change in the propagator, i.e., by a change of the mass. Here, we analyze the effects by taking into account the change of the vector-meson masses using the form

$$m_V(\rho) = m_V \exp(-\alpha_V \rho), \quad (34)$$

where α_V is treated as an adjustable parameter.

On the basis of the SU(3) properties of the ESC model, the changes of vector-meson masses in a nuclear medium induce

the density-dependent effective repulsions in a rather universal manner in NN , YN , and YY channels. Then, our first step is to investigate this effect in usual nuclear matter. Because we expect big cancellations for the scalar exchanges $\epsilon + P$, as well as in the many-body case, we here for simplicity change only the vector-meson masses for an analysis of the sensitivity of, e.g., the well-depths with respect to medium effects.

For convenience, our medium-induced effects are handled in comparison with the three-nucleon interaction (TNI) introduced by Lagaris-Pandharipande [50], which is represented in simple forms of density-dependent two-body interactions. Here, we refer their parameter sets TNI2 and TNI3, reproducing nuclear incompressibility 250 and 300 MeV, respectively. Their TNI is composed of the attractive part (TNA) and the repulsive part (TNR). Our modeling through the change of vector-meson masses corresponds only to their TNR. Hereafter, TNR (TNA) parts of TNI2 and TNI3 are denoted as TNR2 and TNR3 (TNA2 and TNA3), respectively.

In the left panel of Fig. 16, we show the saturation curves of symmetric nuclear matter, namely binding energy per nucleon as a function of ρ , which are obtained from the G -matrix

TABLE XXII. Values of U_Σ at normal density and partial wave contributions for ESC04a–d and NSC97f (in MeV).

	T	1S_0	3S_1	1P_1	3P_0	3P_1	3P_2	D	U_Σ
ESC04a	1/2	11.6	-26.9	2.4	2.7	-6.4	-2.0	-0.8	-36.5
	3/2	-11.3	2.6	-6.8	-2.3	5.9	-5.1	-0.2	
ESC04b	1/2	9.6	-25.3	1.8	1.6	-5.4	-2.1	-0.7	-27.1
	3/2	-9.6	9.9	-5.5	-1.9	5.4	-4.6	-0.2	
ESC04c	1/2	6.4	-20.6	2.4	2.9	-6.7	-1.6	-0.9	-33.2
	3/2	-10.7	6.9	-8.8	-2.6	6.0	-5.8	-0.2	
ESC04d	1/2	6.5	-21.0	2.6	2.4	-6.7	-1.7	-0.9	-26.0
	3/2	-10.1	14.0	-8.5	-2.6	5.9	-5.7	-0.2	
NSC97f	1/2	14.9	-8.3	2.1	2.5	-4.6	0.5	-0.5	-12.9
	3/2	-12.4	-4.1	-4.1	-2.1	6.0	-2.8	-0.1	

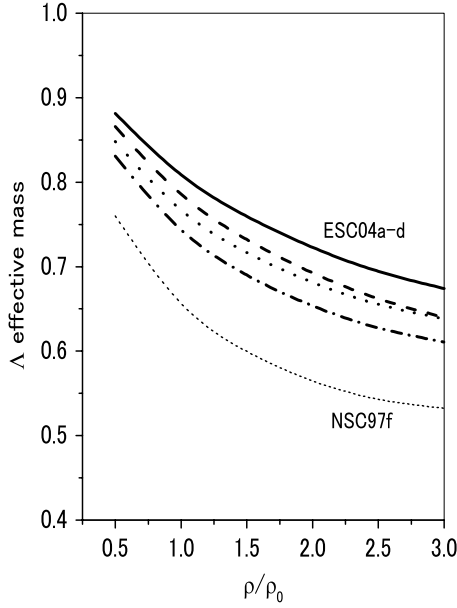


FIG. 14. Calculated values of m_{Λ}^* as a function of ρ/ρ_0 for ESC04a (solid curve), ESC04b (dashed curve), ESC04c (dotted curve), and ESC04d (dot-dashed curve). The thin dashed curve is for NSC97f.

calculations with ESC04 (NN). Here, the upper curve denoted as “QTQ” is calculated with the QTQ prescription. The lower one denoted as “CIES” is obtained with the choice of a continuous intermediate-energy spectrum in the G -matrix equation. The CIES result is known to simulate well the result, including the three-hole line contributions [51]. In the following procedure, however, we use the QTQ result because our G -matrix analyses for hypernuclear systems are based on the QTQ prescription in this article. The box in the figure show the area where nuclear saturation is expected to occur empirically, and the energy minimums of both curves of QTQ and CIES are found to deviate from this area. To realize the nuclear saturation, three-body effects should be added on the contributions of ESC04 (NN) in the same way as the cases of using the other NN interaction models: Here, we use the above mentioned TNI. The dashed curves in the right panel of Fig. 16 are obtained by adding the TNI contributions on the (QTQ) G -matrix results, where the reduction factor 0.8 is multiplied on the TNA part so as to give the energy minimum at an adequate value of $-15 \sim -16$ MeV. The two curves in the figure correspond to the cases of adopting TNI2 and TNI3. Then, the saturation condition is found to be satisfied nicely. Hereafter, when we use the TNI together with ESC04

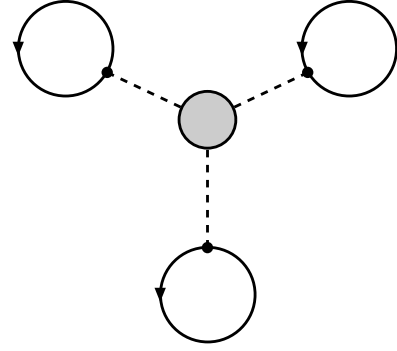


FIG. 15. Triple-meson three-body interaction.

(NN), the factor 0.8 is always multiplied on the TNA part. In addition, the nucleon energy spectra obtained in the case of adopting TNI2 are adopted in the YN G -matrix equations in this work.

Next, we perform the G -matrix calculations with ESC04 (NN) in which the vector-meson masses are changed according to Eq. (32). Hereafter, the medium-corrected versions of ESC04 are denoted as ESC04*(α_V), including the parameter α_V . In the right side of Fig. 16, the two solid curves are obtained by adding the contributions of TNA2 and TNA3 multiplied by 0.8 to the G -matrix results. It should be noted here that the TNR parts are switched off because they are substituted by our medium-induced repulsions. Namely the TNA parts are used here as phenomenological substitutes for the three-body attractive effects that are out of our present scope. The parameter α_V in Eq. (32) is chosen so as to simulate the TNR contributions: The two solid curves in the figure are obtained by choosing $\alpha_V = 0.07 \text{ fm}^3$ and $\alpha_V = 0.18 \text{ fm}^3$, which turn out to be quite similar to the dashed curves obtained by adding the TNI2 and TNI3 contributions, respectively, on the original G -matrix result. Thus, it turns out that the density dependence of our medium-induced repulsion is very similar to that of TNR. Although this similarity is of no fundamental meaning, it is nicely demonstrated that our medium-induced repulsion plays the same role as TNR for nuclear saturation.

Let us study the effects of the medium corrections in the YN sectors of the ESC models. Then, a prospective way is to perform calculations for the values of $\alpha_V = 0.07 \text{ fm}^3$ and $\alpha_V = 0.18 \text{ fm}^3$ that induce repulsions similar to TNR2 and TNR3, respectively, in nucleon matter. In the following analysis, we investigate mainly the case of $\alpha_V = 0.18 \text{ fm}^3$. In Table XXIII, the calculated values of U_{Λ} and U_{Σ} at normal density and their S -state contributions are shown in the case of taking $\alpha_V = 0.18 \text{ fm}^3$. Comparing these values with those in Table XIX

TABLE XXIII. Calculated values of U_{Λ} and U_{Σ} at normal density for ESC04a-d*($\alpha_V = 0.18$). Their S -state contributions are also given. All entries are in MeV.

	$1/2,1 S_0$	$1/2,3 S_1$	U_{Λ}	$1/2,1 S_0$	$1/2,3 S_1$	$3/2,1 S_0$	$3/2,3 S_1$	U_{Σ}
ESC04a*	-12.0	-15.8	-30.6	12.2	-26.4	-11.0	8.6	-27.9
ESC04b*	-11.6	-18.5	-33.0	10.1	-25.5	-9.0	15.2	-19.7
ESC04c*	-12.3	-25.1	-39.3	7.9	-20.0	-10.3	12.7	-23.6
ESC04d*	-12.0	-23.0	-37.2	8.3	-20.3	-9.6	19.1	-16.6

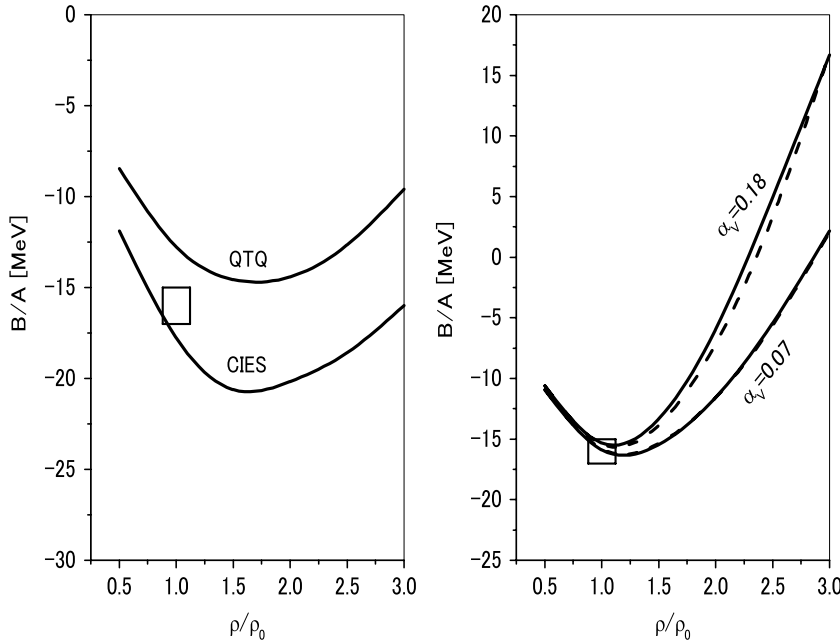


FIG. 16. Binding energy per nucleon B/A in symmetric nuclear matter as a function of ρ/ρ_0 (saturation curve). The box represents the area in which saturation occurs empirically. (Left panel) The two solid curves show the G -matrix results for ESC04 (NN) with the QIQ and CIES prescriptions. (Right panel) The dashed curves are obtained by adding the TNI contributions on the QIQ result, and the solid curves are for the medium-corrected versions ESC04* (NN). See the text for the detail.

and Table XXII, we find that the repulsive contributions are substantial both for U_Λ and U_Σ . In the case of U_Λ , the U_Λ values for ESC04a–d are too attractive in comparison with the empirical indication of $U_\Lambda \sim -30$ MeV. These overbinding values turn out to be improved substantially by our medium-induced repulsion. Especially, the values for ESC04a/b*(α_V) are noted to agree well with the above empirical value. Similar repulsive contributions are seen also in the case of U_Σ , though the resulting values are still negative. However, it is important that the repulsive contribution is large in the 3S_1 ($I = 3/2$) state, as discussed later.

It should be emphasized here that the spin-dependent features of the ΛN G -matrix interaction are not really affected by our medium-induced repulsion. For instance, the values of $U_{\sigma\sigma}(S)$ become small only by 0.05 MeV (ESC04a), 0.09 MeV (ESC04b), 0.10 MeV (ESC04c), and 0.11 MeV (ESC04d) in the case of taking $\alpha_V = 0.18$ fm³. In the cases of the P -state contributions such as $U_{\sigma\sigma}(P)$, $U_{LS}(P)$, and $U_T(P)$, the changes are negligibly small. The change of the effective mass m_Λ^* is also small: The m_Λ^* values for ESC04a–d*($\alpha = 0.18$) are smaller than those for ESC04a–d by only 0.01 \sim 0.02. These facts suggest interesting possibilities of using ESC04a–d*(α_V) in various spectroscopic studies of Λ hypernuclei, where the parameter α_V can be adjusted so as to reproduce experimental values of B_Λ with almost no influence on spin-dependent structures of Λ hypernuclei. Then, we stress that the meaning of the above choice $\alpha_V = 0.18$ fm³ is only for its similarity to TNR3.

Our medium-induced repulsions are related intimately to the problem of maximum masses of neutron stars. As well known, the repulsive three-body force in high-density neutron matter, embodied in TNR, plays an essential role for a stiffening of the EOS of neutron-star matter, assuring the observed maximum mass of neutron stars. However, the hyperon mixing in neutron-star matter brings about the remarkable softening of the EOS, which cancels the effect of the repulsive three-body force for the maximum mass.

To avoid this serious problem, Nishizaki, Takatsuka, and one of the authors (Y.Y.) [52,53] introduced the conjecture that the TNR-type repulsions work universally for YN and YY as well as for NN . They showed that the role of the TNR for stiffening the EOS can be recovered clearly by this assumption. Our model of the medium-induced repulsion explains their assumption quite naturally. In Fig. 17, we draw the values of U_Λ as a function of ρ/ρ_0 in some cases: The three solid curves are for ESC04b and ESC04b*($\alpha_V = 0.07$) and ESC04b*($\alpha_V = 0.18$), and the two dashed curves are obtained by adding the TNR2 and TNR3 contributions on the result for

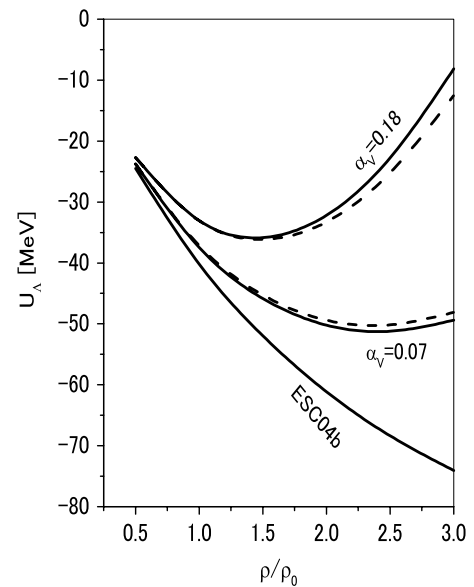


FIG. 17. Calculated values of U_Λ as a function of ρ/ρ_0 . The three solid curves are for ESC04b, ESC04b*($\alpha_V = 0.07$), and ESC04b*($\alpha_V = 0.18$). The two dashed curves are obtained by adding the TNR2 and TNR3 contributions on the result for ESC04b. See the text for the detail.

ESC04b. It is found, here, our medium-induced repulsions for $\alpha_V = 0.07$ and $\alpha_V = 0.18$ are very similar to the TNR2 and TNR3 contributions, respectively, as well as the case of nuclear saturation curves. Thus, it is clearly demonstrated that our medium-induced repulsions, which works universally among octet baryons, will assure the stiffening of the EOS.

In neutron-star matter, the chemical equilibrium condition for Σ^- given by $\mu_{\Sigma^-} = \mu_n + \mu_{e^-}$ makes Σ^- mixing more favorable than Λ mixing controlled by $\mu_{\Lambda} = \mu_n$ in cases of neglecting strong interactions. Then, it is an important problem whether the well depth of Σ^- is attractive or repulsive in neutron matter. As shown in Table XXIII, our medium-induced repulsion for ΣN contributes dominantly in the 3S_1 ($I = 3/2$) state with the largest statistical weight. Thus, this repulsive effect appears most strongly in the Σ^- well depth in neutron matter given by the $I = 3/2$ ΣN interaction.

In our analysis for hypernuclear systems, we do not consider the three-body attraction, such as TNA, which plays an important role for nuclear saturation as well as the three-body repulsion such as TNR and our medium-induced effect. The origin of such a part is considered to be in meson-exchange three-body correlations, being initiated by Fujita-Miyazawa [54]. Possible counterparts in our hyperonic matter will be studied in future.

C. Double- Λ states

Here, we study the $\Lambda\Lambda$ (${}^{11}S_0$) interactions, for which the experimental information can be obtained from the data of double- Λ hypernuclei. In the past, NHC-D [55] has been used popularly as a standard meson-theoretical model for $S = -2$ interactions. The reason was because this interaction is compatible with strong $\Lambda\Lambda$ attraction ($\Delta B_{\Lambda\Lambda} = 4 \sim 5$ MeV) supported by earlier data on double- Λ hypernuclei. This strong $\Lambda\Lambda$ attraction of NHC-D is because of its specific feature that only the scalar singlet meson is taken into account. Because the discovery of NAGARA event identified uniquely as ${}^6_{\Lambda\Lambda}\text{He}$ [56] in 2001, the $\Lambda\Lambda$ interaction is established to be rather less attractive ($\Delta B_{\Lambda\Lambda} \approx 1$ MeV). Then, it is quite important to investigate what values of $\Delta B_{\Lambda\Lambda}$ are obtained for ESC04 models.

Let us here evaluate the values of $\Delta B_{\Lambda\Lambda}({}^6_{\Lambda\Lambda}\text{He})$, taking account of the $\Lambda\Lambda - \Xi N$ coupling effect explicitly. For this purpose, we adopt the three-body model composed of the $\alpha + \Lambda + \Lambda$ and $\alpha + \Xi + N$ configurations. The effective $\Lambda\Lambda - \Lambda\Lambda$ and $\Lambda\Lambda - \Xi N$ interactions [57] are derived in the G -matrix framework as follows: We solve the $\Lambda\Lambda - \Xi N - \Sigma\Sigma$ coupled-channel G -matrix equation for a $\Lambda\Lambda$ pair in nuclear matter, and represent the resultant $\Lambda\Lambda - \Lambda\Lambda$ and $\Lambda\Lambda - \Xi N$ G matrices as local potentials in coordinate space. These G -matrix interactions depend on the nucleon Fermi momentum k_F of nuclear matter. Then, it is a problem what value of k_F should be chosen in our calculation for ${}^6_{\Lambda\Lambda}\text{He}$. In similar calculations for ${}^5_{\Lambda}\text{He}$, the value of k_F parameter included in the ΛN G -matrix interaction was chosen around 1.0 fm^{-1} [58]. This value of $k_F \sim 1.0 \text{ fm}^{-1}$ agree qualitatively with the value derived from the average nuclear density felt by the Λ particle in ${}^5_{\Lambda}\text{He}$. Because a sophisticated estimation of the k_F value is not necessary for our purpose of demonstrating features of

the interaction models, we choose this plausible value of $k_F = 1.0 \text{ fm}^{-1}$ in the present calculations for ${}^6_{\Lambda\Lambda}\text{He}$.

Using our $\Lambda\Lambda - \Lambda\Lambda$ and $\Lambda\Lambda - \Xi N$ G -matrix interactions, three-body variational calculations are performed in the Gaussian basis functions [59], where the $\Xi N - \Xi N$ interaction is not taken into account for simplicity. It should be noted that in our approach high-lying $\Lambda\Lambda - \Xi N - \Sigma\Sigma$ correlations are renormalized into the $\Lambda\Lambda - \Lambda\Lambda$ and $\Lambda\Lambda - \Xi N$ G matrices, and low-lying $\Lambda\Lambda - \Xi N$ correlations are treated in the model space composed of $\alpha + \Lambda + \Lambda$ and $\alpha + \Xi + N$ configurations. To avoid the double counting of the $\Lambda\Lambda - \Xi N$ coupling interaction, it is necessary that the high-lying $\Lambda\Lambda - \Xi N$ correlations are not included in our three-body model space. A practical way for this problem is to take the two Λ (Ξ and N) coordinates from the center of mass of α core, not the relative coordinate between them explicitly, because the short-range correlations are taken into account unfavorably in this model space.

As for the interactions between the α cluster and valence particles (Λ , Ξ , N), we adopt the phenomenological potentials: For $\alpha - \Lambda$ and $\alpha - \Xi$ interactions, we use the two-range Gaussian potentials given in Ref. [57]. Here, the former is fitted so as to reproduce the Λ binding energies of ${}^4_{\Lambda}\text{H}$ and ${}^4_{\Lambda}\text{He}$. The strength of the latter (named as Xa1 [57]) is determined in consideration of the experimental indication that the Ξ well depth is roughly half of the Λ one. However, we use the Kanada-Kaneko potential [60] for the $\alpha - N$ interaction, designed so as to reproduce scattering phase shifts. In the $\alpha + \Xi + N$ channel, we take into account the orthogonality condition between α and N .

In Table XXIV we show the calculated values of $\Delta B_{\Lambda\Lambda}({}^6_{\Lambda\Lambda}\text{He})$ and ΞN admixture probabilities $P_{\Xi N}$ in the cases of using ESC04a-d, NSC97f, and NHC-D. (In the calculation for NHC-D, the hard-core radius in the ${}^{11}S_0$ state is taken as 0.53 fm , and the $\Sigma\Sigma$ channel is not taken into account.) The effect of the medium-induced repulsion is not so remarkable in this case, because the $\Lambda\Lambda$ G matrix is calculated at low density ($k_F = 1.0 \text{ fm}^{-1}$). For instance, the calculated values for ESC04a* ($\alpha = 0.18$) are $\Delta B_{\Lambda\Lambda} = 1.24 \text{ MeV}$ and $P_{\Xi N} = 0.44\%$. The calculated $\Delta B_{\Lambda\Lambda}$ values should be compared with the experimental value $1.01 \pm 0.20^{+0.18}_{-0.11} \text{ MeV}$ [56]. Then, the calculated values for ESC04a-d are considered to be more or less reasonable in the present scope of our simple three-body model.

However, the value of $\Delta B_{\Lambda\Lambda}$ for NSC97f turns out to be rather too small compared with the experimental value: The $\Lambda\Lambda$ interaction of NSC97f is concluded to be too weak. It is interesting that our result for NSC97f is quite similar to the Yamada's result [61], obtained from the sophisticated variational calculation with direct use of NSC97f. This means that our model-space approach with G -matrix effective interactions simulates nicely the real space approach with free-space interactions. It was pointed out by Yamada that the $\Lambda\Lambda - \Xi N - \Sigma\Sigma$ coupling treatment leads to the less $\Lambda\Lambda$ binding than the $\Lambda\Lambda - \Xi N$ one because of the existence of a pseudo bound state in the case of NSC97f. It should be noted that such a pseudo bound state does not appear in the case of ESC04a-d. In Ref. [62] the similar result was obtained for NSC97f by the G -matrix calculation. However, the importance of the rearrangement effect of the α core for $\Delta B_{\Lambda\Lambda}({}^6_{\Lambda\Lambda}\text{He})$

TABLE XXIV. $\Delta B_{\Lambda\Lambda}({}^6\text{He})$ values (in MeV) are calculated with G -matrix interactions derived from ESC04a–d, NSC97, and NHC-D. (The hard-core radius in NHC-D is taken as 0.53 fm.)

	$\Delta B_{\Lambda\Lambda}$ (MeV)	$P_{\Xi N}$ (%)
ESC04a	1.36	0.44
ESC04b	1.37	0.45
ESC04c	0.97	1.15
ESC04d	0.98	1.18
NSC97f	0.34	0.19
NHC-D	1.05	0.14

has been pointed out in Refs. [63–65]. It is an open problem to study core-rearrangement effects on the basis of the ESC04 models.

The most striking feature of ESC04a–d is the far stronger $\Lambda\Lambda - \Xi N$ coupling than NSC97f and NHC-D. In Table XXIV, this feature is seen in larger value of $P_{\Xi N}$ in the case of ESC04a–d. In particular, it is very curious that the $\Lambda\Lambda - \Xi N$ couplings of ESC04c/d are extremely strong. As shown in Ref. [57], such a coupling effect appears dramatically in ${}^5_{\Lambda\Lambda}\text{H}$ and ${}^5_{\Lambda\Lambda}\text{He}$ because of the small energy differences between ground $\Lambda - \Lambda$ states and $\Xi - \alpha$ states. A comprehensive study on the $\Lambda\Lambda - \Xi N$ coupling is now in progress on the basis of ESC04a–d.

D. Properties of ΞN G matrix

There is no ΞN -scattering data at present. We have only uncertain information on Ξ -nucleus interactions experimentally. We consider that the most reliable data in the present stage was given by the BNL-E885 experiment [66], in which they measured the missing mass spectra for the ${}^{12}\text{C}(K^-, K^+)X$ reaction. Reasonable agreement between this data and theory is realized by assuming a Ξ -nucleus potential $U_{\Xi}(\rho) = -V_0 f(r)$ with well depth $V_0 \sim 14$ MeV within the Wood-Saxon (WS) prescription.

Let us here derive the potential energies U_{Ξ} using the G -matrix theory in the same way as the cases of U_{Λ} and U_{Σ} . In the past, NHC-D gave rise to attractive values of U_{Ξ} , whereas strongly repulsive values were obtained for the other Nijmegen models. Then, it is very curious what values of U_{Ξ} are obtained for ESC04a–d.

In the same way as in the ΣN case, we solve the ΞN starting channel G -matrix equation in the QTQ prescription. Likewise, the Ξ conversion width Γ_{Ξ} , because of an energy-conserving $\Xi N - \Lambda\Lambda$ transition, is not calculated here. In this case, the channel-coupling treatments are performed for $\Lambda\Lambda - \Xi N - \Sigma\Sigma$ and $\Xi N - \Lambda\Sigma - \Sigma\Sigma$ channels.

In Table XXV we show the calculated values of U_{Ξ} at normal density and their partialwave contributions for ESC04a–d and ESC04d* ($\alpha_V = 0.18$). For comparison, the result for NHC-D is also given, where the hard-core radii are taken as 0.50 fm in all channels and the $\Sigma\Sigma$ and $\Lambda\Sigma$ channels are not taken into account. Now, the remarkable difference among ESC04a–d is revealed: These four versions turn out to give rise to completely different values of U_{Ξ} . It should be noted that the ESC models such as ESC04c/d can bring about

TABLE XXV. Values of U_{Ξ} at normal density and partial wave contributions for ESC04a–d and ESC04d* ($\alpha_V = 0.18$). For comparison, the result for NHC-D is also shown (hard-core radii are taken as 0.50 fm in all channels.). All entries are in MeV.

	T	1S_0	3S_1	1P_1	3P_0	3P_1	3P_2	U_{Ξ}
ESC04a	0	8.1	-10.0	1.0	-0.3	-0.4	-0.7	
	1	-4.5	21.8	-0.7	0.7	-0.1	0.3	+15.1
ESC04b	0	5.9	-2.4	0.7	0.7	1.0	-0.4	
	1	0.5	27.9	0.6	0.9	-0.3	1.2	+36.3
ESC04c	0	5.9	-15.7	1.2	-0.1	-1.8	-1.2	
	1	6.8	1.9	-0.8	0.1	-0.3	-1.7	-5.5
ESC04d	0	6.4	-19.6	1.1	1.2	-1.3	-2.0	
	1	6.4	-5.0	-1.0	-0.6	-1.4	-2.8	-18.7
ESC04d*	0	6.3	-18.4	1.2	1.5	-1.3	-1.9	
	1	7.2	-1.7	-0.8	-0.5	-1.2	-2.5	-12.1
NHC-D	0	-4.5	2.6	-1.8	-0.2	-0.6	-1.7	
	1	0.2	5.3	-2.6	0.0	-2.9	-5.6	-11.9

attractive Ξ -nucleus potentials predicting the existence of Ξ hypernuclei. It is very interesting that ESC04d*, including the medium-induced repulsion, leads to the Ξ well depth similar to the above “experimental” value. Though the attractive value of U_{Ξ} is obtained also in the case of NHC-D, its partial-wave contribution is completely different from those in the case of ESC04c/d. In the former case, the attractive U_{Ξ} is owing to the strong P -state attraction. In the latter case, however, the strong attraction in the ${}^{13}S_1$ state plays an essential role for it. Because of this reason, various Ξ hypernuclear states will be predicted even in light s -shell systems on the basis of ESC04c/d. Level structures of these Ξ states have to reflect the peculiar spin and isospin dependences of the underlying ΞN interactions. The detailed analysis will be given in our next article.

XI. DISCUSSION AND CONCLUSIONS

We have shown in this article that the ESC approach to the nuclear force problem is able to make a connection between on the one hand the presently available baryon-baryon data and on the other hand the underlying quark structure of the baryons and mesons. Namely a successful description of both the NN - and YN -scattering data is obtained with meson-baryon coupling parameters that are almost all explained by the QPC model. This at the same time in obedience of the strong constraint of no bound states in the $S = -1$ systems. Therefore, the ESC04 models of this article are an important step in the determination of the baryon-baryon interactions for low-energy scattering and the description of hypernuclei in the context of broken $SU(3)$ symmetry. The values for many parameters, which in previous work were considered to free to large extend, are now limited strongly, and tried to be made consistent with the present theoretical view on low-energy hadron physics. This is in particularly the case for the $F/(F + D)$ ratios of the MPE interactions. These ratios for the vector- and scalar-mesons are rather close to the QPC-model predictions. This holds also for the values of

the coupling constants. Here, the introduction of a zero in the form factor is important, leading to a sizable reduction in the scalar couplings. It is interesting that the features of σ exchange with a zero in the form factor are very similar to those obtained in a chiral unitary approach [67].

The application of the $Q\bar{Q}$ -pair creation to baryon-meson couplings using a 3S_1 model [68] for pseudoscalar and vector-meson couplings, and the nucleon-nucleon interactions has first been attempted by Fujiwara and Hecht [69]. We did not explore this possibility, but it is not unlikely that this alternative leads to a similar scheme of couplings as the 3P_0 model.

The G -matrix results show that basic features of hypernuclear data are reproduced nicely by ESC04, improving some weak points of the soft-core OBE models NSC89 [3] and NSC97 [4]. In spite of this superiority of ESC04 for hypernuclear data, perhaps not every aspect of the effective (two-body) interactions in hypernuclei can be described by this model. For example, this could be the case for the well depth U_Σ . From the results it is clear that a good fit to the scattering data not necessarily means success in the G -matrix results. To explain this one can think of two reasons: (i) the G -matrix results are sensitive to the two-body interactions below 1 fm, whereas the present YN -scattering data are not, (ii) other than two-body forces play an important role. However, since the $NN \oplus YN$ fit is so much superior for ESC04 than for OBE-models, we are inclined to look for solutions to the mentioned problems outside the two-body forces. A natural possibility is the presence of 3BFs in hypernuclei which can be viewed as generating effective two-body forces, which could

solve the well-depth issues. In the case of the $\Delta B_{\Lambda\Lambda}$ also 3BF could be operating. This calls for an evaluation of the 3BFs NNN , ΛNN , ΣNN , $\Lambda\Lambda N$, etc., for the soft-core ESC model, consistent with its two-body forces.

The ΛN p waves seem to be better, which is the result of the truly simultaneous $NN + YN$ fitting. This is also reflected in the better K_Λ value, making the well-known small spin-orbit splitting smaller.

Finally, we mention the extensive work on baryon-baryon interactions using the resonating group method (RGM), exploiting quark-gluon exchange (QGE) in conjunction with OBE, taking full account of the antisymmetrization of the six quarks in the two-baryon systems [70]. A remarkable difference with the ESC models is that QGE leads to strong repulsion in the $\Sigma N({}^3S_1, I = 3/2)$ - and the $\Sigma N({}^1S_0, I = 1/2)$ channels. In contrast, in this article we have assumed that QGE is very suppressed dynamically.

ACKNOWLEDGMENTS

We thank Professor T. Motoba for many stimulating discussions and Professor D. E. Lansky and Dr. A. Dieperinck for useful comments. Th.A.R. is very grateful for the generous hospitality extended to him in the fall of 2004 at the Osaka-EC University, where part of the final work on this article was done. Y.Y. thanks IMAPP of the Radboud University Nijmegen for its hospitality. He is supported by the Japanese Grant-in-Aid for Scientific Research Fund of Education, Culture, Sports, Science and Technology (No. 16540261).

-
- [1] T. A. Rijken, Phys. Rev. C **73**, 044007 (2006).
 [2] T. A. Rijken and Y. Yamamoto, Extended-soft-core Baryon-Baryon Model, III Hyperon-Nucleon Scattering $S = -2$, 2006 (in preparation).
 [3] P. M. M. Maessen, Th. A. Rijken, and J. J. de Swart, Phys. Rev. C **40**, 2226 (1989).
 [4] T. A. Rijken, V. G. J. Stoks, and Y. Yamamoto, Phys. Rev. C **59**, 21 (1999).
 [5] T. A. Rijken, Ann. Phys. (NY) **164**, 1, 23 (1985).
 [6] T. A. Rijken, in *Few-Body Problems in Physics '99*, Proceedings of the 1st Asian-Pacific Conference, August 23–28, Tokyo, edited by S. Oryu, M. Kamimura, and S. Ishikawa (Springer-Verlag, New York, 2000), p. 317.
 [7] T. A. Rijken, Nucl. Phys. **A691**, 322c (2001).
 [8] L. Micu, Nucl. Phys. **B10**, 521 (1969); R. Carlitz and M. Kislinger, Phys. Rev. D **2**, 336 (1970).
 [9] Y. Yamamoto and H. Bandō, Prog. Theor. Phys. **83**, 254 (1990).
 [10] T. Motoba and Y. Yamamoto, Nucl. Phys. **A585**, 29c (1995).
 [11] T. Hasegawa *et al.*, Phys. Rev. Lett. **74**, 224 (1995).
 [12] R. H. Dalitz and F. von Hippel, Phys. Lett. **10**, 153 (1964).
 [13] M. M. Nagels, T. A. Rijken, and J. J. de Swart, Ann. Phys. (NY) **79**, 338 (1973).
 [14] J. J. de Swart, Rev. Mod. Phys. **35**, 916 (1963); **37**, 326(E) (1965).
 [15] P. A. Carruthers, *Introduction to Unitary Symmetry* (Wiley, New York, 1966).
 [16] R. E. Marshak, Riazuddin, and C. P. Ryan, *Theory of Weak Interactions in Particle Physics* (Wiley, New York, 1969).
 [17] T. A. Rijken and V. G. J. Stoks, Phys. Rev. C **54**, 2869 (1996); **54**, 2869 (1996).
 [18] A. Le Yaouanc, L. Oliver, O. Pène, and J.-C. Raynal, Phys. Rev. D **8**, 2223 (1973); **11**, 1272 (1975).
 [19] M. Chaichain and R. Kögerler, Ann. Phys. (NY) **124**, 61 (1980).
 [20] M. M. Nagels, T. A. Rijken, and J. J. de Swart, Phys. Rev. D **17**, 768 (1978).
 [21] R. A. Bryan and A. Gersten, Phys. Rev. D **6**, 341 (1972).
 [22] V. G. J. Stoks, R. A. M. Klomp, M. C. M. Rentmeester, and J. J. de Swart, Phys. Rev. C **48**, 792 (1993).
 [23] R. A. M. Klomp (private communication).
 [24] J. K. Ahn *et al.*, Nucl. Phys. **A761**, 41 (2005); H. Kanda (private communication).
 [25] V. G. J. Stoks and T. A. Rijken, Nucl. Phys. **A613**, 311 (1997).
 [26] G. Alexander, U. Karshon, A. Shapira, G. Yekutieli, R. Engelmann, H. Filthuth, and W. Lughofer, Phys. Rev. **173**, 1452 (1968).
 [27] B. Sechi-Zorn, B. Kehoe, J. Twitty, and R. A. Burnstein, Phys. Rev. **175**, 1735 (1968).
 [28] F. Eisele, H. Filthuth, W. Fölsch, V. Hepp, E. Leitner, and G. Zech, Phys. Lett. **B37**, 204 (1971).
 [29] R. Engelmann, H. Filthuth, V. Hepp, and E. Kluge, Phys. Lett. **21**, 587 (1966).
 [30] V. Hepp and M. Schleich, Z. Phys. **214**, 71 (1968).
 [31] D. Stephen, Ph.D. thesis, University of Massachusetts, 1970; Z. Phys. **214**, 71 (1968).
 [32] J. J. de Swart and C. Dullemond, Ann. Phys. **19**, 458 (1962).

- [33] J. J. de Swart, M. M. Nagels, T. A. Rijken, and P. A. Verhoeven, Springer Tracts Mod. Phys. **60**, 138 (1971).
- [34] Y. Fujiwara, T. Fujita, C. Nakamoto, and Y. Suzuki, Prog. Theor. Phys. **100**, 957 (1998).
- [35] ESC04 *YN* potentials, see <http://nn-online.org>.
- [36] B. Sakita and K. C. Wali, Phys. Rev. **139**, B1355 (1965).
- [37] E. Hiyama, M. Kamimura, T. Motoba, T. Yamada, and Y. Yamamoto, Phys. Rev. C **65**, 011301(R) (2001).
- [38] A. Nogga, H. Kamada, and W. Glöckle, Phys. Rev. Lett. **88**, 172501 (2002).
- [39] H. Nemura, Y. Akaishi, and Y. Suzuki, Phys. Rev. Lett. **89**, 142504 (2002).
- [40] D. J. Millener, Nucl. Phys. **A691**, 93c (2001).
- [41] R. R. Scheerbaum, Nucl. Phys. **A257**, 77 (1976).
- [42] E. Hiyama, M. Kamimura, T. Motoba, T. Yamada, and Y. Yamamoto, Phys. Rev. Lett. **85**, 270 (2000).
- [43] Y. Fujiwara, M. Kohno, K. Miyagawa, and Y. Suzuki, Phys. Rev. C **70**, 047002 (2004).
- [44] Y. Yamamoto, S. Nishizaki, and T. Takatsuka, Prog. Theor. Phys. **103**, 981 (2000).
- [45] C. J. Batty, E. Friedman, and A. Gal, Prog. Theor. Phys. Suppl. **117**, 227 (1994).
- [46] J. Dabrowski, Phys. Rev. C **60**, 025205 (1999).
- [47] H. Noumi *et al.*, Phys. Rev. Lett. **89**, 072301 (2002).
- [48] M. Kohno, Y. Fujiwara, Y. Watanabe, K. Ogata, and M. Kawai, Prog. Theor. Phys. **112**, 895 (2004).
- [49] A. D. Jackson, Annu. Rev. Nucl. Part. Sci. **33**, 105 (1983); A. D. Jackson, E. Krotcheck, and M. Rho, Nucl. Phys. **A407**, 495 (1983).
- [50] I. E. Lagaris and V. R. Pandharipande, Nucl. Phys. **A359**, 349 (1981).
- [51] M. Baldo, A. Fiasconaro, H. Q. Song, G. Giansiracusa, and U. Lombardo, Phys. Rev. C **65**, 017303 (2002).
- [52] T. Takatsuka, S. Nishizaki, and Y. Yamamoto, *Proceedings of the International Symposium on Perspectives in Physics with Radiactive Isotopes*, Hayama, Kanagawa, Japan, Nov. 13–16, 2000 [Eur. Phys. J. A **13**, 213 (2002)].
- [53] S. Nishizaki, Y. Yamamoto, and T. Takatsuka, Prog. Theor. Phys. **105**, 607 (2001); **108**, 703 (2002).
- [54] J. Fujita and H. Miyazawa, Prog. Theor. Phys. **17**, 360 (1957); **17**, 366 (1957).
- [55] M. M. Nagels, T. A. Rijken, and J. J. deSwart, Phys. Rev. D **15**, 2547 (1977).
- [56] H. Takahashi *et al.*, Phys. Rev. Lett. **87**, 212502 (2001).
- [57] D. E. Lansky and Y. Yamamoto, Phys. Rev. C **69**, 014303 (2004).
- [58] Y. Yamamoto and H. Bandō, Prog. Theor. Phys. Suppl. **81**, 9 (1985).
- [59] Y. Yamamoto, H. Takaki, and K. Ikeda, Prog. Theor. Phys. **82**, 13 (1989).
- [60] H. Kanada, T. Kaneko, S. Nagata, and M. Nomoto, Prog. Theor. Phys. **61**, 1327 (1979).
- [61] T. Yamada, Phys. Rev. C **69**, 044301 (2004).
- [62] I. Vidaña, A. Ramos, and A. Polls, Phys. Rev. C **70**, 024306 (2004).
- [63] M. Kohno, Y. Fujiwara, and Y. Akaishi, Phys. Rev. C **68**, 034302 (2003).
- [64] Q. N. Usmani, A. R. Bodmer, and B. Sharma, Phys. Rev. C **70**, 061001(R) (2004).
- [65] H. Nemura, S. Shinmura, Y. Akaishi, and Khin Swe Myint, Phys. Rev. Lett. **94**, 202502 (2005).
- [66] P. Khaustov *et al.*, Phys. Rev. C **61**, 054603 (2000).
- [67] E. Oset, H. Toki, M. Mizobe, and T. T. Takahashi, Prog. Theor. Phys. **103**, 351 (2000).
- [68] Y. W. Yu and Z. Y. Zhang, Nucl. Phys. **A426**, 557 (1984).
- [69] Y. Fujiwara, Prog. Theor. Phys. **88**, 933 (1992), and the references cited here.
- [70] Y. Fujiwara, T. Fujita, M. Kohno, C. Nakamoto, and Y. Suzuki, Phys. Rev. C **65**, 014002 (2002), and cited references.